



UPPSALA  
UNIVERSITET

TVE MFE 19006

Examensarbete 30 hp  
Juni 2019

# FORCE PREDICTION AND ESTIMATION FOR A POINT ABSORBER WAVE ENERGY CONVERTER

---

Zahra Shahroozi



UPPSALA  
UNIVERSITET

Teknisk- naturvetenskaplig fakultet  
UTH-enheten

Besöksadress:  
Ångströmlaboratoriet  
Lägerhyddsvägen 1  
Hus 4, Plan 0

Postadress:  
Box 536  
751 21 Uppsala

Telefon:  
018 – 471 30 03

Telefax:  
018 – 471 30 00

Hemsida:  
<http://www.teknat.uu.se/student>

## Abstract

# **FORCE PREDICTION AND ESTIMATION FOR A POINT ABSORBER WAVE ENERGY CONVERTER**

*Zahra Shahroozi*

The ocean is one of the greatest untapped renewable energy sources on earth, where a wave energy converter (WEC) may be used to extract a substantial amount of energy and convert it into electricity.

However, for WECs to be economically competitive with other renewable resources a number of challenging engineering problems must be dealt with. Power maximizing is one way to reduce its Levelized Cost of Energy (LCOE) compared to established energy resources. This can be achieved by tuning a real-time control system of the WEC according to the instantaneous incident wave, for which the future knowledge of excitation force or wave elevation is required in order to make the control problem causal. This research investigates the methodologies to estimate and predict the excitation to be used in CorPower Ocean (CPO) WEC control system.

An Auto-Regressive (AR) model is used to predict the excitation force for a required prediction horizon based on only its past history. The required horizon length is computed by the effect of suboptimal velocities, i.e. replacing the full noncausal reference transform function by truncated versions in the convolution with excitation force. To create the history for the AR model, a Kalman Filter with Harmonic Oscillator (KFHO) estimates the excitation force based on a simple WEC model and measured values for position and velocity of the WEC.

The accuracy of the predicted signal compared to the measured signal is presented for two different time horizons. The results display that the performance of the predictor/estimator is highly dependent on the predictor parameters and the optimum number of frequencies which identifies the dynamic of the excitation force. The proposed method of combined prediction and estimation has shown around 96.6% and 99.4% accuracy compared to filtered estimated force as well as 79.9% and 77.6% accuracy compared to measured excitation force for prediction horizons of 5 seconds and 2.5 second respectively.

keywords: Control System, Excitation Force

Handledare: Jørgen Hals Todalshaug  
Ämnesgranskare: Jens Engström  
Examinator: Irina Temiz  
ISSN: 1650-8300, UPTEC ES19 006

# SAMMANFATTNING

---

Havet är en av de största outnyttjade förnybara energikällorna på jorden, där ett vågkraftverk (Wave Energy Converter, WEC) kan användas för att extrahera en betydande mängd energi och omvandla den till el. För att en WEC ska vara ekonomiskt konkurrenskraftig med andra förnybara energikällor måste dock ett antal utmanande tekniska problem hanteras. Att maximera effektuttaget är ett sätt att minska energikostnaden (Levelized Cost Of Energy, LCOE) jämfört med etablerade energikällor. Detta kan uppnås genom att ställa in ett realtidsstyrningssystem enligt den momentana inkommande vågen, för vilken den framtida kunskapen om excitationkraft eller våghöjd är nödvändig för att göra kontrollproblemet kausal. Denna forskning undersöker metoderna för att uppskatta och förutsäga excitationen som ska användas i CorPower Ocean (CPO) WEC-styrssystemet.

En auto-regressiv (AR) -modell används för att förutsäga excitationkraften för en nödvändig förutsägelseshorisont baserad på endast dess tidigare historia. Den erforderliga tidshorisonten beräknas genom påverkan av suboptimala hastigheter, dvs att ersätta den fullständiga icke-kausala referenstransformfunktionen med trunkerade versioner i faltningen med exciterande kraft. För att skapa historiken för AR-modellen uppskattar ett Kalman-filter med harmonisk oscillator (KFHO) excitationkraften baserat på en enkel WEC-modell och uppmätta värden för position och hastighet för WEC:en.

Noggrannheten hos den förutspådda signalen jämfört med den uppmätta signalen presenteras för två olika tidshorisonter. Resultaten visar att prestanda för prediktorn / estimatorn är starkt beroende av prediktorparametrarna och det optimala antalet frekvenser som identifierar dynamiken hos excitationkraften. Den föreslagna metoden för kombinerad förutsägelse och uppskattning har visat omkring 96,6% och 99,4% noggrannhet jämfört med filtrerad uppskattad kraft samt 79,9% och 77,6% noggrannhet jämfört med uppmätt excitationkraft för prediktionshorisonter på 5 sekunder respektive 2,5 sekunder.

Nyckelord: Styrssystem, Excitationkraft

# ACKNOWLEDGEMENTS

---

I would like to express my deep and sincere gratitude to my supervisor, Jørgen Hals Todalshaug, Lead scientist of CorPower Ocean Company for his invaluable guide throughout this research, and I am deeply inspired by his dynamism, sincerity, and motivation. I like to thank my subject reader, Jens Engström, senior lecturer at Uppsala University, for his support who always incentivize me forward during my thesis work.

I owe considerable gratitude and thanks to Malin Göteman, senior lecturer at Uppsala University, who introduced me to this exciting field of science when participating on her lectures in wave energy technology course. And I felt greater passion towards Wave Energy Concept after working under her supervision and gained invaluable experiences and knowledge.

I am particularly grateful, to my previous co-supervisor and friend, Marianna Giassi, Ph.D. student at Uppsala University, who further inspired me in wave energy by her engineering brilliance.

I am grateful to CorPower for giving me the opportunity to write my master thesis with them, where, not only did I learn and acquire immeasurable knowledge and experiences but also, I met wonderful friends and colleagues.

I want to thank Uppsala University for these two wonderful years where I was able to develop my knowledge deeper and gave me the chance to meet my precious friends. Many thanks to all my friends in Uppsala that I cannot imagine my time without them.

I am pleased to thanks Juan de Santiago, senior lecturer and student counselor at Uppsala University, for his patience, and unfailing support in these two years.

I want to thank my parents and my brother and express my gratefulness to them for their unconditional support, and encouragement. That for me is the greatest honor to be their daughter and sister. And the last but not the least, huge thanks to my husband, Reza, for his unceasing love, support, encouragement, patience, and motivation.

Zahra Shahroozi

# NOMENCLATURE

---

<i>Symbol</i>	<i>Description</i>
$\tilde{S}(f)$	Spectral Density as a function of frequency
$H_s$	Significant Wave Height
$T_e$	Energy Period
$v_{opt}$	Optimal Velocity for maximum energy extraction
$B$	Radiation Resistance
$K_f$	Friction corresponds to losses in the system
$H_{opt}$	Transfer function between excitation force and velocity
$h_{opt}$	Impulse response of transfer function
$J_{\phi^*}$	Cost function of AR Predictor
$\phi^*$	Regression coefficient of AR Predictor
$z_k$	Observation vector at time k for Kalman Filter
$S_k$	System state vector at time k for Kalman Filter
$\hat{S}_{k i}$	Estimation of $S$ at time $k$ based on time $i$ , $k \geq i$ for Kalman Filter
$P_k$	Covariance matrix of Kalman Filter
$A$	State transition matrix of Kalman filter
$G$	Weighting matrix for state error of Kalman Filter
$w_k$	Process (or system, or plant) noise vector of Kalman Filter
$v_k$	measurement noise covariance matrix of Kalman Filter
$Q_k$	Process (or system, or plant) noise covariance matrix of Kalman Filter
$R_k$	Measurement noise covariance matrix of Kalman Filter
$K$	Kalman gain matrix
$v_3$	Buoy velocity in heave motion
$\eta_3$	Buoy position in heave or vertical axis
$\xi_3$	Water elevation in heave axis

---

## *Table of Contents*

<b>ABSTRACT</b>	<b>2</b>
<b>SAMMANFATTNING</b>	<b>3</b>
<b>ACKNOWLEDGEMENTS</b>	<b>4</b>
<b>NOMENCLATURE</b>	<b>5</b>
<b>1 INTRODUCTION</b>	<b>9</b>
1.1 Wave Energy Conversion	9
1.2 CorPower Ocean Wave Energy Converter	9
1.3 Prediction Horizon	10
1.4 Prediction of Excitation Force	11
1.5 Estimation of Excitation Force	12
1.6 Research Questions	13
1.7 Limitations and Assumptions for this Study	13
<b>2 THEORY</b>	<b>14</b>
2.1 Ocean Waves	14
2.1.1 Linear Wave Theory	14
2.2 Wave Device Intercation	15
2.2.1 General Motion of the Buoy	15
2.2.2 Hydrodynamic Forces	16
2.2.3 Equation of Motion	17
2.3 CorPower Ocean Concept	21
2.3.1 Power Take Off (PTO)	21
2.3.2 WaveSpring	22
2.3.3 Gas spring	23
2.3.4 Cascade gearbox	23
2.4 Prediction Horizon	24
2.4.1 Frequency Domain Model	24
2.4.2 Time Domain Model	25
2.5 Prediction of Excitation Force	25
2.5.1 Autoregressive	25
2.5.2 Accuracy of Prediction	26

2.6	Estimation of Excitation Force	27
2.6.1	Kalman Filter	27
<b>3</b>	<b>METHODS</b>	<b>31</b>
<hr/>		
3.1	Information Flow from Measurement to Predicted Signal	31
3.2	WEC Model	31
3.3	Prediction Horizon	32
3.4	Prediction of Excitation Force	35
3.4.1	Filtering the excitation force	35
3.4.2	Coherence Time	37
3.4.3	AR Optimization	37
3.4.4	Numerical Computation of AR Coefficients	38
3.5	Estimation of Excitation Force	38
3.5.1	Linearization of Non-Linear Forces	38
3.5.2	Validation of linear system	43
3.5.3	Kalman Filter Approaches	44
3.6	Combining Prediction and Estimation of Excitation Force	45
<b>4</b>	<b>RESULTS</b>	<b>46</b>
<hr/>		
4.1	Prediction Horizon	46
4.2	Prediction of Excitation Force	46
4.3	Estimation of Excitation Force	48
4.4	Combining Prediction and Estimation of Excitation Force	52
<b>5</b>	<b>DISCUSSION</b>	<b>54</b>
<hr/>		
5.1	Prediction Horizon	54
5.2	Prediction of Excitation Force	54
5.3	Estimation of Excitation Force	54
5.4	Combining Prediction and Estimation of Excitation Force	55
<b>6</b>	<b>CONCLUSION</b>	<b>56</b>
<b>7</b>	<b>FUTURE WORK</b>	<b>57</b>
<hr/>		
7.1	Prediction Horizon	57
7.2	Prediction of Excitation Force	57
7.3	Estimation of Excitation Force	57

<b>REFERENCES</b>	<b>58</b>
<b>APPENDIX A</b>	<b>60</b>
<b>APPENDIX B</b>	<b>61</b>

---

# 1 INTRODUCTION

## 1.1 Wave Energy Conversion

Tremendous amount of energy contained in the ocean waves motivated mankind to think about and develop ideas to harvest and use this seemingly everlasting source of energy. There are, however, more steps to be taken to make these ideas economically viable which involves challenging design problems on a range of engineering disciplines. Maximizing the amount of output energy that a wave energy converter can provide, is crucial for reducing its LCOE (levelized cost of energy). An important feature is the ability to control the motion of the converter according to the instantaneous wave conditions. The aim of this research is to estimate and predict the excitation force for the time horizon that is needed to use real time control algorithms on CorPower Ocean’s wave energy converter, and thereby to maximize the power output under varying wave conditions.

## 1.2 CorPower Ocean Wave Energy Converter

CorPower Ocean (CPO) is one of the leading companies in the merging wave energy industry. Their technology is expected to achieve a Levelized Cost of Energy (LCOE) that is competitive with established energy sources. CPO has developed a wave energy converter (WEC) that is inspired by the pumping principle of the human heart, supported by 30 years of research. This WEC is manufactured as light weighted system with higher natural frequency of oscillation compared to similar heavier WEC which is made to resonate by means of the WaveSpring control system, which can be detuned in storms condition for its survival.

The unique technological features which makes CorPower stand out among its competitors are for instance the cascade gearbox, i.e. a new patent developed by CorPower Ocean company, as well as WaveSpring technology. Comparing WaveSpring technology and latching phase control (common control strategy in Wave Energy Technology), WaveSpring provides similar power capture amplification with less than half machinery force which makes PTO more cost effective. And also, a significant reduction in size of the buoy has been made compared to the conventional gravity balanced WEC without phase control. WaveSpring technology increased the annual average power output of point absorber by more than 300%. This step-change not only improves the performance but also provides the device with minimum cost and complexity.

All these advantages places CPO in a route to introduce the world’s first certified, warranted and bankable WECs for large scale array deployment by 2023. Figure 1 and Figure 2 illustrate the five product verification stages of CPO from 2012 to 2022.



Figure 1 Structured product verification in five Stages.

Retrieved May 26, 2019 from <https://www.etipocean.eu/assets/Uploads/1-CorPower-Ocean-Patrik>



Figure 2 Different stages of WEC at CPO.

Retrieved May 26, 2019 from <https://www.etipocean.eu/assets/Uploads/1-CorPower-Ocean-Patrik>

### 1.3 Prediction Horizon

Accurate future knowledge of wave elevation, excitation force or WEC state would be necessary to attain optimal control system of a WEC in polychromatic sea states. The control approach for WEC is mainly designed by tuning the system in frequency domain to regulate the dynamical system of WEC, for being in resonant with incoming waves, to extract the maximum energy at each peak frequency of wave spectra. Although the optimal frequency relationship can provide us with the real time optimal control, the problem rises by converting it to the time domain which resulted in noncausal<sup>1</sup> transfer function for which the knowledge of future will be essential to understand the condition for optimal power absorption [3]. Now, the questions are what would be the length of time on which future knowledge is required? And how can this prediction time horizon be computed? To answer these questions, different authors present different solution and suggestion to achieve this prediction time horizon. Falnes [12] suggests the radiation memory, i.e. the time on which the radiation force and thus wave radiated which is affected by past motion, defines the required prediction horizon. Justino [6] emphasizes the importance of sea state that the radiation memory will develop. Clement [6] notes natural period of the WEC plays an important role in defining the prediction horizon. Price et al [6] recommend the importance of distinguishing computed prediction horizon using gathered local information compared to gathered remote information. Moreover, they introduce and develop the concept of premonition time i.e. difference between required and available knowledge of future signals, and emphasizes the fact that two factors, geometry of the device and sea state, highly influence computing the premonition time. And last but not the least, Korde et al [3] note that the required prediction horizon can be found by computing the effect of suboptimal velocities, i.e. replacing the full noncausal reference transform function by truncated versions in the convolution with excitation force.

As most of the above authors mention, the sea state is important in developing the memory kernel which plays a main role to dictate the required future knowledge; therefore, what would be the role of the sea state in computation of the prediction time horizon? Price et al [6] answer this question by introducing two main scenarios. One theoretical scenario which includes two extreme cases and then real sea state scenario which contains two real sea cases.

In the first scenario, two theoretical conditions have been considered; one when the velocity is sinusoidal and the other when the velocity is a white noise. In the first case, the sinusoidal velocity

---

<sup>1</sup> In a noncausal system, output variables at the present time can be influenced by the input variables of the future values.

is resulted from sinusoidal wave elevation with zero bandwidth. The velocity can be computed regardless of what the duration of the memory kernel by sinusoidal extrapolation is. As a result, it can be expressed that since the available information is infinite due to sinusoidal pattern of wave elevation or velocity, the prediction time horizon is zero. Second case is completely in contrast with the first case and the chance of this case in real sea state is either seldom or non. Future knowledge is impossible to compute by using the sinusoidal extrapolation since the bandwidth of the white noise is infinite. Hence, the future knowledge can be obtained by duration of the memory kernel to design optimal control system. Therefore, it can be said that when there is no available knowledge from velocity pattern or incoming wave, the prediction horizon would be the duration of the required information.

In the second scenario, by defining the coherence time as the time which the signal can be modeled by sinusoidal extrapolation while autocorrelation of the signal in time domain is above the considered threshold, two real cases have been investigated. These two cases are closer to real sea state since it is neither extreme sinusoidal nor extreme white noise. One case with a long coherence time of velocity and other with a short coherence time of velocity. In the case of long coherence, optimal control can be achieved by sinusoidal extrapolation. In other words, when the coherence time of the velocity is longer than the duration of memory kernel, no future knowledge would be required. However, in second case, the coherence is not long enough to provide us with required knowledge. It can represent that when there is deficiency in available knowledge compared to required knowledge and information, the remote monitoring will be needed.

In this work, the method used to compute prediction horizon has been set based on Falnes [5], Korde et al [3] and Price [6] ideology, by taking careful consideration of all possible approaches introduced by above mentioned authors.

## 1.4 Prediction of Excitation Force

As it is stated in the previous section, regarding the importance of real time prediction of the free surface elevation, wave excitation force, or WEC states to formulate and design the optimal noncausal control system, several methods for prediction of future knowledge depending on operation principle of the devices, control strategy of each device, and available instrumentation have been introduced. Now the question might rise that considering early stage of control and signal and system, one might design control algorithm for which the need of future knowledge would not be a key point for designing an optimal control system of the device. So why should we go into trouble of predicting the future? The work in [19] and [22] suggest the control algorithm which disregards the need for future knowledge, however, for maximizing the power in most of the real sea states acquiring the knowledge of the future excitation force or surface elevation is still essential, owing to noncausality of the optimal PTO force. So, once more the indisputable fact of need of future knowledge is emphasized.

Several prediction models and methods have been developed based on two following main approaches, i.e. recommended to predict the future knowledge for short term waves. In the first approach the excitation force or wave elevation can be predicted, based only on local single-point measurement, in which there is no need to consider radiated and diffracted waves or multi-directional waves. The first approach is also called “looking backward” methods since by using only past measurements at the point of interest and then treating wave elevation or excitation force as time series predicts the future wave elevation or excitation force. In second approach prediction of excitation force or wave elevation can be accomplished by installing several measurement devices in arrays and reconstruct the wave field based on installed measurement devices around

the point of interest, [4], [3], [23]. The second approach is called “looking forward”, which predicts the wave elevation and excitation force by using models for physical or stochastic propagation of the waves. Following these two approaches, Mérigaud [23] proposed undefined framework for prediction of wave elevation, on which both measured and predicted wave elevation are treated as Gaussian vector which enfold both “looking forward” and “looking backward” approaches. There are other prediction methods such as autoregressive (AR) [24], [25], the autoregressive moving average [24], [26], [27], the Kautz method [27], and Neural Networks [24] which are classified differently depending on their performance.

The main interest in this work is to predict the excitation force directly to be able to compute the WEC power output, and based on that calculate the optimal damping of generator and its torque to be set as the input of control system to tune the system in a way to absorb all the energy possible (considering device capacity) from available energy that is provided by the ocean.

The autoregressive method has been chosen as a solution to predict the excitation force by considering the first approach, “looking backward”. Therefore, the prediction of excitation force is accomplished based on single local measurement at point of interest and considering only its past history. AR is a simple and at the same time accurate model to predict the excitation force for low frequency waves (swell), which are the most energetic waves. Moreover, in contrast with neural network, the inherent characteristics can be easily analyzed through analytical calculation [3], [28]. Furthermore, by comparing AR with ARMA, the latter introduces more complex solution with fairly similar result as AR, which is compared and proved in [4]. In the end, the AR method is assigned as the foremost choice of this work, recalling all its advantages.

## 1.5 Estimation of Excitation Force

The continual estimation of excitation force in real time would be indispensable in order to calculate the prediction horizon, i.e. introduced in previous chapter, and furthermore to design optimal control system to get some steps closer from possible energy that one WEC can extract towards available energy that is available by the ocean (Budal diagram, Appendix A).

A large number of the estimation strategies is outlined and compared in [11]. For instance, convolution with predicted wave elevation estimation strategy, CPWE, estimates the excitation force based on convolution product between the wave elevation and the excitation force impulse response, that is used in [15] and [16]; in Kalman filter (KF) with random walk estimation, KFRW, two alternative setups are considered, one taking excitation force as an unknown input to the system, and two using motion measurement device and observer to estimate excitation force at each time step by taking a random step away from the previous value; Kalman filter with harmonic oscillator estimation strategy, KFHO, is considered the most common estimator approach for heaving point absorber device, i.e. also used in [2], [17], and [18], which has the same working process as KFRW with the difference of using a Kalman filter in conjunction with a harmonic oscillator (HO) to model the dynamics of excitation force; In the extended Kalman filter harmonic oscillator, EKFO, not only is the instantaneous frequency of excitation force calculated, but also the instantaneous amplitude of the excitation force is computed [19], and [20]. In receding horizon estimation, RHE, the same way as KFRW, KFHO, and EKFO the excitation force is considered an unknown input and in contrast to the mentioned estimators no dynamical model is assumed, i.e. the authors in [21] believe that eluding the dynamical model for excitation force amends the obtained results. The last estimator but not the least is the pressure acceleration displacement strategy which estimates the excitation force by using pressure measurement over wetted surface of the device [15]. Following the research and investigation of the theory behind

each above-mentioned estimator, Kalman filter with harmonic oscillator have been chosen as the base of the current work.

The excitation force is estimated through measurement of other variables that are highly influenced by excitation force such as position and velocity of the WEC. The Kalman filter with harmonic oscillator (KFHO) has been chosen as a solution to estimate the excitation force on the WEC according to its measured position and velocity. The estimation is updated by combining a set of observation or measurements which is further discussed in the theory section.

Now the question might rise, why Kalman filter with harmonic oscillator? To answer this question, one can summarize its features as follows; [8]

- Being **unbiased** filter estimator meaning that  $E[\hat{F}_{exc}] = E[F_{exc}]$ ; the expectation of its output is the expectation of the quantity being estimated.
- Recall that it is considered as the **minimum variance unbiased estimator (MVUE)**. Since it minimizes the mean square error during the posteriori process by adding the measurement information that is well described further on in theory section.
- Kalman filter is classified as the most accurate linear filter both over time varying and time invariant filter applications due to displaying the **linear** minimum variance of error filter. [8]
- Furthermore, it can be categorized as close loop estimator due its dynamical system of estimator which provides it with higher capability for handling the uncertainty and noise.

## 1.6 Research Questions

The main research questions in this work can be formulated as;

- What is the required time horizon to predict the excitation force for optimal noncausal control system?
- How can the excitation force be predicted within the specified horizon? What is the accuracy of this prediction?
- How can the excitation force be estimated based on other system variables?

## 1.7 Limitations and Assumptions for this Study

The framework of this study is defined by the following assumption and limitation to answer the research questions;

- Linear potential theory is taken to define the equation of motion by assuming fluid is irrotational, incompressible, and non-viscous.
- This study considers the excitation force only in heave direction.
- The nonlinear forces that are introduced by Power Take Off (PTO) system must be linearized to be used in dynamical system of Kalman filter with harmonic oscillator. The nonlinear forces are assumed as spring-damper forces and are linearize by Tylor expansion and equivalent viscous damping accordingly. The linearization is further explained in Linearization of Non-Linear Forces.
- In the WEC model used for this study, the braking force is disregarded for sake of simplification.

## 2 THEORY

---

### 2.1 Ocean Waves

#### 2.1.1 Linear Wave Theory

Navier-Stokes equations are nonlinear partial derivative equations that describe the motion of a viscous fluid, and they are derived by applying fundamental physical laws of momentum, mass, and energy conservation.

To derive the simplified form of Navier-Stokes equation, three theorems are considered; [32]

- I. Continuity equation; (Mass conservation)

$$\frac{\partial \rho}{\partial t} + \bar{\nabla} \cdot (\rho \bar{u}) = 0 \quad (2.1)$$

Where  $\bar{u}$  is the velocity of fluid, and  $\rho$  is the fluid density.

- II. Transport theorem;

$$\frac{d}{dt} \iiint_V \rho f dV = \iiint_V \rho \left( \bar{u} \cdot \bar{\nabla} f + \frac{\partial f}{\partial t} \right) dV \quad (2.2)$$

Where  $f(\bar{x}(t), t)$  is any function, and  $V$  is the volume.

- III. Incompressible fluid;

$$\bar{\nabla} \cdot \bar{u} = 0 \quad (2.3)$$

Hence, the simplified Navier-Stokes equation is;

$$\frac{\partial u}{\partial t} + \bar{u} \cdot \bar{\nabla} \bar{u} = -\frac{1}{\rho} \bar{\nabla} p + \nu \Delta \bar{u} + \frac{1}{\rho} \bar{f}_{ext} \quad (2.4)$$

The left-hand side of the equation expresses the acceleration of the fluid, and the right-hand side describes the total force per unit mass.

In general, Navier-Stokes equations are extremely difficult to solve, i.e. considered as one of the Millennium problems, defined by Clay mathematics Institute. A simpler solution can be achieved through a set of assumptions for the fluid that is analyzed in a wave energy concept. [32]

- I. Irrotational fluid,  $\bar{\nabla} \times \bar{u} = 0$ .
- II. Incompressible,  $\bar{\nabla} \cdot \bar{u} = 0$
- III. Ideal fluid, i.e. viscosity can be neglected
- IV. The external force acting on the fluid is gravity,  $\bar{f}_{ext} = \nabla(-\rho g)$

These assumptions simplify the Navier-Stokes equation to Laplace equation together with boundary constraints. Hence, fluid velocity potential ( $\phi$ ) satisfies Laplace equation as;

$$\bar{\nabla}^2 \phi = 0 \quad (2.5)$$

This equation can be solved assuming harmonic (regular) wave. Due to linearity of the linear potential theory, irregular waves can be constructed from superposition of harmonic waves that are solutions to the Laplace equation. [32]

Ocean waves are modeled as irregular waves consisting of several harmonic waves with different angular frequency and waves amplitude and have the following definitions. [32]

### Spectral Density

The spectral density function is proportional to the energy density of each wave component of the  $w_n$ . And it can be expressed as follows;

$$\int_0^{\infty} S(\omega)d\omega = \int_0^{\infty} S(2\pi f)2\pi df = \int_0^{\infty} \tilde{S}(f)df \quad (2.6)$$

### Spectral Moment

Furthermore, the  $n$ th spectral moment is defined by the spectral density function and wave frequency;

$$m_n = \int_0^{\infty} f^n \tilde{S}(f)df \quad (2.7)$$

### Energy Period

The energy period of the irregular wave is defined as the period of a harmonic wave that has the same energy content as the irregular wave;

$$T_e = \frac{m_{-1}}{m_0} \quad (2.8)$$

### Significant Wave Height

In irregular waves the significant wave height is the defined with the following equation;

$$H_s = 4\sqrt{m_0} \quad (2.9)$$

## 2.2 Wave Device Intercation

### 2.2.1 General Motion of the Buoy

In general, the buoy motion can be described by 6 degree of freedom in motion three movement and three rotation around x, y, and z axis, as it is shown in Figure 3. These 6 degrees of freedom are surge, sway, heave, roll, pitch and yaw. The mathematical model of this work is mainly based on heave motion of the buoy.

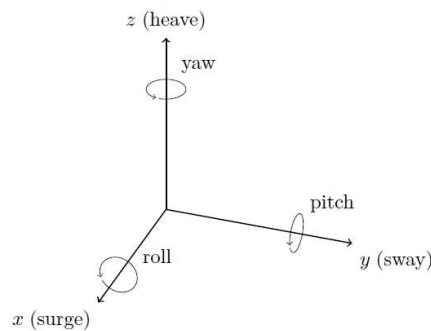


Figure 3 General motion of the buoy

## 2.2.2 Hydrodynamic Forces

In order to understand the buoy and wave interaction, it is of utmost importance to study the forces from the wave that act on the buoy. With the assumptions of linear potential wave theory that were described in the previous section, the hydrodynamic force acting on the buoy consists of;

$$F_{hyd} = F_{hyst} + F_{rad} + F_{exc} + F_{drag} \quad (2.10)$$

These forces are summarized in Table 1 and each one is further elaborated in the following sections.

Table 1 Hydrodynamic and hydrostatic forces

Name	Abbreviation	Description
Hydrostatic force	$F_{hyst}$	Net effect of gravity and buoyancy
Radiation force	$F_{rad}$	Due to radiated outgoing waves
Excitation force	$F_{exc}$	Due to incident wave
Drag force	$F_{drag}$	Due to pressure in CorPower concept <sup>2</sup>

### 2.2.2.1 Hydrostatic Force

While the gravity and hydrostatic force cancel each other out at the equilibrium position of the buoy, it is common to define the hydrostatic force as buoyancy stiffness times the position of the buoy from the equilibrium position;

$$F_{hys} = \rho g V \eta_3 \quad (2.11)$$

### 2.2.2.2 Radiation Force

The oscillating body creates radiated waves by its movement. Therefore, radiation force can be defined as a function of the geometry of the oscillating body. In frequency domain we have;

$$v_3 = \dot{\eta}_3 \quad (2.12)$$

$$\hat{F}_{rad}(\omega) = (B(\omega) + i\omega m_a(\omega))v_3(\omega) \quad (2.13)$$

Where  $B(\omega)$  is the resistance, and  $m_a(\omega)$  is called the added mass both related to the geometry of the buoy.

### 2.2.2.3 Excitation Force

The force that transfers motion, i.e. energy, to the buoy due to the incident wave.

$$F_{exc}(\omega) = \hat{f}_{exc}(\omega)\hat{\zeta}_w(\omega) \quad (2.14)$$

---

<sup>2</sup> Drag forces in CorPower application are mostly pressure related and friction related drag can be neglected.

Where  $\hat{\zeta}_w$  is the wave elevation, the complex  $\hat{f}_{exc}$  is given by its  $abs(\hat{f}_{exc})$ , i.e. amplitude of the excitation force, and  $arg(\hat{f}_{exc})$  gives phase shift between incoming wave and excitation force. Note that excitation force  $F_{exc}$  represents the complex form.

### 2.2.2.4 Drag Force

The drag force is related to the velocity of the buoy in heaving motion as;

$$F_{drag} = \frac{1}{2} C_{D3} \rho A_{WP} v_3 |v_3| \quad (2.15)$$

Where  $C_{D3}$  is the drag coefficient in heave direction,  $A_{WP}$  is the water plane area of the buoy, and  $v_3$  is the heaving velocity of the buoy.

## 2.2.3 Equation of Motion

### 2.2.3.1 Equation of Motion in Time Domain

Presuming the linear potential theory (small wave elevation and motion, inviscid and irrotational flow), equation of motion will be introduced as follows; [9]

$$m_{osc} \dot{v}_3 = F_{exc} + F_{\nabla} + F_g + F_d + F_R + F_b + F_m \quad (2.16)$$

where,  $F_{exc}$  is the excitation force from incident waves,  $F_{\nabla}$  is the buoyancy force,  $F_g$  is the gravity force,  $F_d$  is the hydrodynamic drag force,  $F_R$  is the radiation force,  $F_b$  is the braking force (which is zero here),  $F_m$  is the machinery force,  $m_{osc}$  is the oscillating mass,  $v_3 = \dot{\eta}_3$  is the heave velocity of WEC and following that  $\dot{v}_3$  is heave acceleration of the WEC. To have a better overview of the above equation, its parameters have been broken down as follows; [9]

- The oscillating mass;

$$m_{osc} = m_b + m_{\infty} + T_{gb}^2 J_g \quad (2.17)$$

where

- The buoyancy force;

$$F_{\nabla} = \rho g V_{sub} \quad (2.18)$$

where the submerged volume in equilibrium position is;

$$V_{sub} = V_{eq} - A_{wp} \eta_3 \quad (2.19)$$

where,  $V_{eq}$  is equilibrium volume,  $A_{wp}$  is water plane area, and  $\eta_3$  is buoy position i.e. time variant.

- Gravity force;

$$F_g = -m_b g \quad (2.20)$$

- Drag force;

$$F_D = -\frac{1}{2} A_3 C_{D3} \rho (v_3 - \dot{\xi}_3) |v_3 - \dot{\xi}_3| \quad (2.21)$$

where  $\zeta_3$  is the buoy position,  $A_3$  is the amplitude in heave direction, and  $C_{D3}$  is the drag coefficient in heave direction.

- Braking force;

$$F_b = 0; \quad (2.22)$$

In this system study, the braking force is disregarded, hence the braking force consider as zero.

- The radiation force due to radiated waves (added mass and damping) is defined;

$$F_R = -m_\infty \dot{v}_3(t) - \int_{-\infty}^t k_{33}(t-\tau) v(\tau) d\tau \equiv -m_\infty \dot{v}_3(t) - F_r(t) \quad (2.23)$$

- Here, the  $m_\infty$  is added mass and  $F_r$  is the convolution term referred to the radiation force. The convolution term can be expressed by state space model;

$$\dot{z}(t) = A_r z(t) + B_r v_3(t) \quad (2.24)$$

$$F_r = C_r z(t) \quad (2.25)$$

where  $z$  is the radiation model's state vector,  $A_r$ ,  $B_r$ ,  $C_r$  are the system, input and output matrices respectively.

- The full machinery force can be written as below by considering following assumptions;

$$F_m = F_p + F_{WS} + F_l, gb + T_{gb} (\tau_{gen} + \tau_{l, mech}) \quad (2.26)$$

- By assuming machinery is infinitely stiff, further on the generator speed can be derived as direct function of the buoy heave velocity.
- The generator speed is;

$$\omega_{gen} = T_{gb} v_3 \quad (2.27)$$

where  $\omega_{gen}$  is generator speed and  $T_{gb}$  is gearbox modulus;

where  $u_g$  is conversion ratio in the gearbox which relates forces across gearbox. Radius of pinion in gear box which relates velocities across gear box.

- Moreover, the oscillating mass expressed as summation of buoy mass, added mass and equivalent inertia of the rotating equipment;

$$m_{osc} = m_b + m_\infty + T_{gb}^2 J_g \quad (2.28)$$

where  $J_g$  is gearbox inertia.

- In machinery equation,  $F_p$  is the pretension force which is computed according to the gas pressure  $p_p$  inside the pretension cylinder;

$$F_p = -(p_p - p_{atm})A_p + F_{l,p} = -(p_p - p_{atm})A_p - (N_{0,p} + C_{p,p} p_p) f_{c,p} \frac{v_3}{|v_3|} - C_{v,p} v_3 \quad (2.29)$$

where  $p_{0,p}$  is the initial pressure inside pretension module,  $V_{0,p}$  is the initial pretension volume,  $c_{v,p}$  is the viscous pretension coefficient,  $f_{c,p}$  is the friction coefficient for coulomb coefficient,  $N_{0,p}$  is the total contact force of squeeze seal, and  $p_{atm}$  is the atmospheric pressure.

- Wave spring force,  $F_{WS}$ , is computed according to the gas pressure  $p_{WS}$  inside the WaveSpring cylinder as well as taking into account the number of cylinders  $N_{WS}$ :

$$\begin{aligned} F_{WS} &= N_{WS} T_{r2WS} F_{WS,axial} = \\ &N_{WS} T_{r2WS} [(p_{WS} - p_{atm}) A_{WS} + F_{l,WS}] = \\ &N_{WS} T_{r2WS} \left[ (p_{WS} - p_{atm}) A_{WS} - (N_{0,WS} + C_{p,WS} p_{WS}) f_{c,WS} \frac{v_3}{|v_3|} - C_{v,WS} v_3 \right] \end{aligned} \quad (2.30)$$

And wave spring modulus;

$$T_{r2W} = \frac{\eta_3}{\sqrt{l_0^2 + \eta_3^2}} \quad (2.31)$$

Where  $\gamma$  is adiabatic thermodynamic property,  $A_{WS}$  is the rod area in wave spring,  $N_{0,WS}$  is the total contact force of squeeze seal,  $f_{c,WS}$  is the friction coefficient for coulomb coefficient.

Now, the force that corresponds to the gearbox and its loss is explained briefly.

- Gearbox loss  $F_{l,gb}$  is expressed as;

$$F_{l,gb} = -(N_{0,gb} + |F_{gb}|) f_{c,gb} \frac{v_3}{|v_3|} \quad (2.32)$$

Where  $N_{0,gb}$  is the total contact force of squeeze seal,  $f_{c,gb}$  is the friction coefficient for the Coulomb force.

- And  $F_{gb}$  is simplified as below;

$$F_{gb} \approx T_{gb} \tau_{gen} \quad (2.33)$$

Where  $T_{gb}$  is gearbox modulus and  $\tau_{gen}$  is generator torque.

- The last expression in machinery force is expressed as;

$$F_{MGL} = T_{gb} (\tau_{gen} + \tau_{l,mech}) \quad (2.34)$$

Here since generator torque,  $\tau_{gen}$ , is considered as zero due to simplification, the above equation represents mechanical generator force loss,  $F_{MGL}$ , and  $\tau_{l,mech}$  is the mechanical generator loss.

### 2.2.3.2 Equation of Motion in Frequency Domain

The force-velocity model in frequency domain is expressed as;

$$j\omega M V(\omega) + Z_r(\omega) V(\omega) + \frac{K_s}{j\omega} V(\omega) + K_f V(\omega) = F_{exc}(\omega) + F_{PTO}(\omega) \quad (2.35)$$

where  $F_{PTO}$  is the PTO force that consists of machinery and braking force,  $F_{exc}$  is the wave excitation force,  $V(\omega)$  is the velocity in frequency domain, and  $K_s$  is the stiffness coefficient, which results from the imbalance between gravity and hydrostatic restoring force. The friction coefficient  $K_f$  represents the losses in transmission, pretension module, generator axis and drag, and  $Z_r(\omega)$  is the radiation impedance due to waves radiated by body's motion and can be decomposed as;

$$Z_r(\omega) = B(\omega) + j\omega[M_a(\omega) + M_\infty] \quad (2.36)$$

Where  $B(\omega)$ , is the radiation resistance which is a real and even function in the frequency domain, consequently, the corresponding time domain impulse response function is also real and even. And  $M_a$  is the added mass less its high-frequency limit,  $M_\infty$ , which will then cancel out the singularity at infinite frequency.

#### 2.2.3.2.1 Friction terms

To model friction forces, the well-known Stribeck friction curve, i.e. combination of the Coulomb, Stribeck and viscous friction component, has been used, see Appendix B. As a result, the friction related to the losses can be computed from friction parameter or friction force of the PTO system;

$$R_p = f_{p,c,v} + f_{p,N_0} + f_{p,c,N} P_{0,p} f_{p,f,c} \frac{4}{A\pi\omega} \quad (2.37)$$

$R_p$  represents corresponding loss of the pretension module,  $f_{p,c,v}$  is the pretension viscous friction coefficient,  $f_{p,N_0}$  is the pretension nominal pressure friction coefficient,  $f_{p,c,N}$  is the pretension friction dependent to the pressure coefficient,  $P_{0,p}$  is the nominal pretension pressure,  $f_{p,f,c}$  is the Columbus friction coefficient of pretension, and the  $A$  is the nominal oscillation amplitude.

$$R_t = f_{gb,c,v} + f_{gb,N_0} f_{gb,f,c} \frac{4}{A\pi\omega} \quad (2.38)$$

$R_t$  is the transmission losses,  $f_{gb,c,v}$  is the gearbox viscous friction coefficient,  $f_{gb,N_0}$  is the nominal gearbox friction coefficient,  $f_{gb,f,c}$  is the Columbus friction coefficient of gearbox, and the  $A$  is the nominal oscillation amplitude.

$$R_{gen} = u_{r,p}^2 \left( f_{gen,c,v} + f_{gen,N_0} f_{gen,f,c} \frac{4}{A\pi\omega} \right) \quad (2.39)$$

$R_{gen}$  is the generator axis losses,  $f_{gen,c,v}$  is the generator viscous friction coefficient,  $f_{gen,N_0}$  is the generator nominal friction coefficient,  $f_{gen,f,c}$  is the Columbus friction coefficient of generator,  $u_{r,p}$  is the pin speed of the generator, and  $A$  is the nominal oscillation amplitude.

$$R_d = \frac{8}{3} \times 0.5\rho C_{D3} A_{WP} \frac{\omega}{A\pi} \quad (2.40)$$

$R_d$  is the drag loss,  $C_{D3}$  is the drag coefficient in heave direction,  $A_{wp}$  is the water plan area,  $\rho$  is the sea water density and  $A$  is the nominal oscillation amplitude.

And  $\omega$  is the derived from energy period of the sea state considering its spectral density i.e. calculated from surface elevation.

Therefore,  $K_f$  can be calculated as;

$$K_f = R_p + R_t + R_d + R_{gen} \quad (2.41)$$

## 2.3 CorPower Ocean Concept

Hereby, different components of CPO technology are outlined.

### 2.3.1 Power Take Off (PTO)

CorPower Oceans wave energy converter can be separated into three parts, mooring i.e. connected to the seabed, the buoy that floats with wave elevation, and the PTO i.e. installed inside the buoy. The pretension module is placed between the PTO module and the mooring cable to pull the buoy down and establish the equilibrium floating position. The PTO consists of a rack, a gearbox, a horizontal shaft, gas spring, and two generators. Since PTO is fixed to the buoy, the buoy and the PTO as well as the rack oscillate with each other. The relative motion along the PTO and the rack is transferred to the horizontal shaft and make it rotate inside the gearbox and eventually runs the generators [29]. Figure 4, illustrates pretension module and different components inside the buoy hall of CPO's WEC.

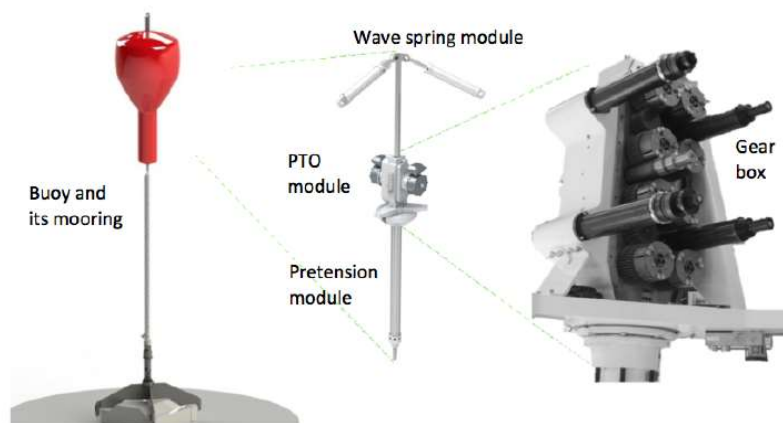


Figure 4 CorePower's wave energy converter. Reproduced from [29]

### 2.3.2 WaveSpring

Wave spring consists of gas springs connected between the buoy hull and the center rod. A negative spring<sup>3</sup> arrangement in WaveSpring technology provides phase control that increases the bandwidth of point absorbers. The negative spring modules work directly on the linear motion of the buoy to avoid the losses i.e. caused by large energy flows through the PTO system [30]. Figure 5 displays the WaveSpring's cylinders and pressurized chamber inside the buoy hull.

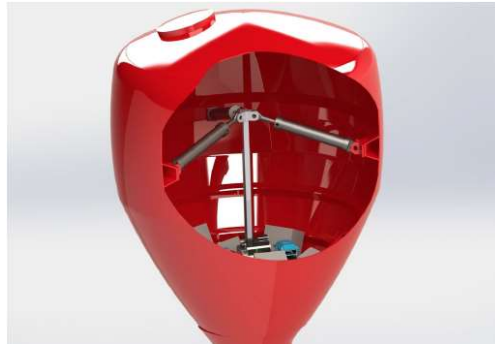


Figure 5 WaveSpring chamber. Reproduced from [29]

Cylinders with pressurized chamber neutralize the hydrostatic forces. In natural position the net of WaveSpring forces is zero, meaning that the gas spring forces cancel out each other. While, when the buoy leaves the equilibrium position, the axial component of forces points out towards the displacement. The wave spring forces increases the oscillation amplitudes even higher than the amplitude of wave elevation [29]. Figure 6 demonstrate the effect of WaveSpring force on displacement of the buoy.

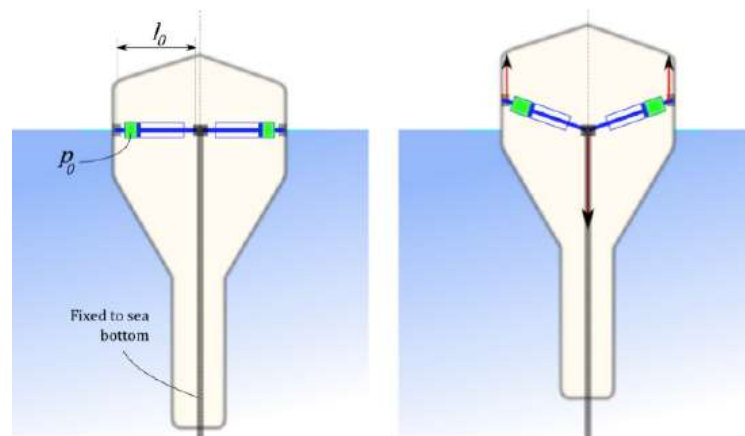


Figure 6 effect of negative spring on displacement of the buoy. Reproduced from [29]

---

<sup>3</sup> "Positive spring results in a stabilizing force; so, moving away from the equilibrium position causes a force towards the equilibrium. A negative spring does the opposite: moving away from the center causes a destabilizing force away from the center."

<http://www.wavepowerconundrums.com/>

### 2.3.3 Gas spring

Another gas spring is connected axially between the buoy and the center rod to provide a pretension force that allocates the buoy at its midpoint.

### 2.3.4 Cascade gearbox

The cascade gearbox is designed for transferring the linear to rotating motion with high persistence. Also, it provides high power density while distributing the large load to multiple small gears. Furthermore, damping the transient load makes the device very robust. The most benefit of this technology is to transmit high loads during the high speeds in lightweight package while keeping the efficiency in high level. The most important feature of the cascade gearbox is to increase the speed rather to decrease it. The cascade gearbox consists of one rack in middle and eight pinion gears, four on each side of the rack [31]. Figure 7 and Figure 8 show the different elements of the CPO's cascade gearbox.

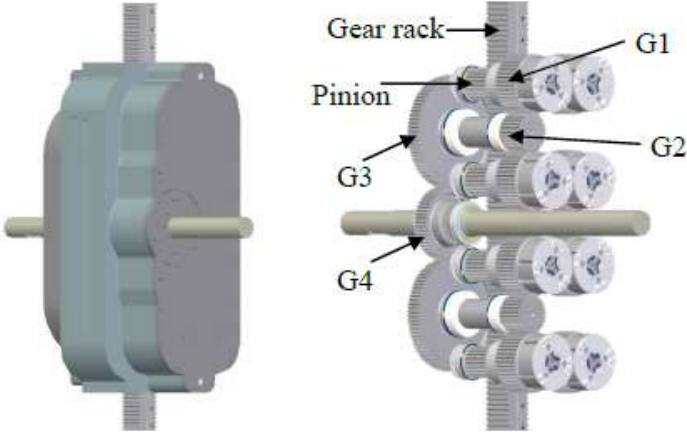


Figure 7 cascade CorPower with cover (left) and without (right). Reproduced from [31]

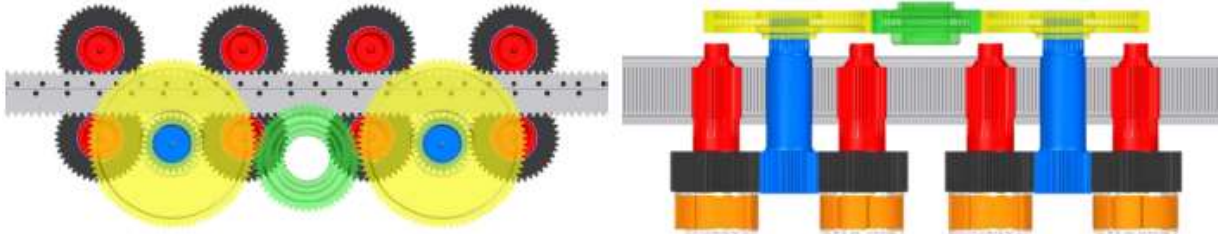


Figure 8 cascade gearbox. the rack (grey) is transferred power to the eight pinions (red). A flex unit (orange) and a shaft is transmitting power to the G1 gears (black) and then to the G2 gears (blue), then power is transferred via a shaft to the G3 gears (yellow). Finally, power is transferred to the G4 gear (green). Reproduced from [31]

## 2.4 Prediction Horizon

Hereby, the system has been discussed both from frequency domain and time domain point of view to investigate further why the knowledge of future for real time optimal control is needed and how the time length on which future knowledge is required can be computed.

### 2.4.1 Frequency Domain Model

The frequency domain technique is the significant approach to rise the system productivity and step on closer to its economic viability. Although this technique would not be applicable to design optimal control on wave-by-wave basis, the real time control in the current stage involves the frequency domain relationship to regulate the system to be tuned for absorbing maximum energy. Hence, it emphasizes the importance of understanding the model in the frequency domain.

#### 2.4.1.1 Analysis of the System in Frequency Domain

Referring to Equation of Motion in Frequency Domain, the optimal velocity giving maximum energy extraction can be derived considering a compact way to describe the force-velocity equation in frequency domain;

$$(F_{PTO} + F_{exc}) \frac{1}{Z_i(\omega)} = V(\omega) \quad (2.42)$$

where the  $Z_i(\omega)$  is the intrinsic impedance. It can be defined as follows;

$$Z_i(\omega) = Z_r + K_f + j\omega M + \frac{K_s}{j\omega} \quad (2.43)$$

Following extensive study in [5] and further review in [3], the maximum wave energy that is transferred from the wave to the PTO can be explained when;

$$F_{PTO} = -Z_i^*(\omega)V(\omega) \quad (2.44)$$

where  $Z_i^*(\omega)$  is the complex conjugate of the intrinsic impedance of the system. For optimal power absorption the impedance provided by the PTO should be equal to the complex conjugate of intrinsic impedance at each frequency to provide the system with the desired amplitude and phase.

The maximum energy extraction can be derived in an alternative and equivalent way by phase and amplitude control, i.e. the relation between oscillation velocity and wave excitation force for which the friction of the system has been taken into consideration; [3]

$$V(\omega) = \frac{1}{Z_i(\omega) + Z_i^*(\omega)} F_{ex}(\omega) = \frac{1}{2B(\omega) + 2K_f} F_{ex}(\omega) \quad (2.45)$$

The optimal velocity in frequency domain is then expressed as follows; [3]

$$V_{opt} = \frac{1}{2B(\omega) + 2K_f} F_{ex}(\omega) = H_{opt}(\omega)F_{ex}(\omega) \quad (2.46)$$

The maximum average absorbed power, through consideration of the above criteria, would be equal to half of the average excitation power, while the other half will be lost in wave radiation.

## 2.4.2 Time Domain Model

Analyzing system from time domain point of view is crucial in order to understand why future knowledge is required to design an optimal control system, and what is the role of memory kernel in that regards. [3]

### 2.4.2.1 Analysis of Noncausality in Time Domain

Following explanation on frequency domain model section,  $V_{opt}$  can be written in time domain; [3]

$$v_{opt}(t) = \int_{-\infty}^t h_{opt}(\tau) f_{exc}(t - \tau) d\tau \quad (2.47)$$

This integration introduces the noncausality in calculation of  $v_{opt}$  through  $f_{exc}(t - \tau)$  term which represents the future knowledge of excitation force.

$h_{opt}(t)$  is the inverse Fourier transform of  $H_{opt}(\omega)$ ;

$$h_{opt}(t) = \mathcal{F}^{-1} \left\{ \frac{1}{2B(\omega) + 2K_f} \right\} = \mathcal{F}^{-1} \{ H_{opt}(\omega) \} \quad (2.48)$$

If  $\omega \rightarrow \infty$  in equation above the radiation resistance goes to zero, so  $H_{opt}(\omega)$  tends to a constant value of the  $1/2K_f$ . Therefore, it can be written as;

$$h_{opt}(t) = \mathcal{F}^{-1} \{ K_{opt}(\omega) \} + \frac{1}{2K_f} \delta(t) = \frac{1}{2K_f} \delta(t) + k_{opt}(t) \quad (2.49)$$

$$K_{opt}(\omega) = H_{opt}(\omega) - \frac{1}{2K_f} \quad (2.50)$$

Note that from the noncausality point of view,  $h_{opt}(t)$ ,  $k_{opt}(t)$  have the same characteristics, as they differ only at time  $t = 0$ .  $h_{opt}(t)$  is real and even since the Fourier transform is real and even and tend to zero for infinite time while Fourier transform tends to constant value for  $\omega = 0$ . [3]

## 2.5 Prediction of Excitation Force

### 2.5.1 Autoregressive

An autoregressive model will be used to forecast the excitation force based on its available history. It assumes that the excitation force at time constant  $k$  is linearly related with a number  $p$  of its past values, which is also called the model order number. The weighting coefficients of this linear relation are trained on  $N$  number of time steps based on minimizing a cost function.

#### 2.5.1.1 AR Model

The future value of the excitation force is calculated based on its past values as follows; [4]

$$\hat{F}_{exc k|k-1} = F_{ex k-1}^* \phi^* \quad (2.51)$$

where  $\hat{F}_{exc_k|k-1}$  is the predicted excitation force and the  $F_{exc_{k-1}}^*$  is the vector of the pervious excitation force values;

$$F_{exc_{k-1}}^* = \begin{bmatrix} F_{exc_{k-1}} & F_{exc_{k-2}} & \dots & F_{exc_{k-p}} \end{bmatrix} \quad (2.52)$$

and  $\phi^*$  is a vector containing all the regression coefficient as,

$$\phi^* = \begin{bmatrix} \phi_1 & \phi_2 & \dots & \phi_p \end{bmatrix}^T \quad (2.53)$$

The model coefficients are identified by the least squares (LS) method which minimizes the quadratic error between the predicted and real values;

$$J_{\phi^*} = \sum_{i=p+1}^N \left( F_{exc_i} - \hat{F}_{exc_i|i-1} \right)^2 \quad (2.54)$$

where N is also called the number of past values on which the model is trained. [4]

Therefore, the coefficients that minimize the cost function are identified as; [4]

$$\phi^* = \left( Z_{1,N-1}^T Z_{1,N-1} \right)^{-1} \left( Z_{1,N-1}^T K_{p+1,N} \right) \quad (2.55)$$

Where  $Z_{1,N-1} \in \mathbb{R}^{(N-p-1) \times p}$ ;

$$Z_{1,N-1} = \begin{bmatrix} F_{exc_p} & F_{exc_{p-1}} & \dots & F_{exc_2} & F_{exc_1} \\ F_{exc_{p+1}} & F_{exc_p} & \dots & F_{exc_3} & F_{exc_2} \\ \vdots & \vdots & \ddots & \vdots & \vdots \\ F_{exc_{N-1}} & F_{exc_{N-2}} & \dots & F_{exc_{N-p+1}} & F_{exc_{N-p}} \end{bmatrix} \quad (2.56)$$

And  $K_{p+1,N} \in \mathbb{R}^{(N-p-1) \times p}$  as;

$$K_{p+1,N} = \begin{bmatrix} F_{exc_{p+1}} & F_{exc_{p+2}} & \dots & F_{exc_{N-1}} & F_{exc_N} \end{bmatrix}^T \quad (2.57)$$

## 2.5.2 Accuracy of Prediction

Accuracy of the prediction is defined by a Goodness-of-fit (GOF) where the quadratic error between the real  $F_{exc}$  and predicted one  $\hat{F}_{exc}$  is computed for each time instance. Then, the average is taken for the whole time series.

$$GoF = \frac{\sum_{k=t_0}^{t_{end}} \left( 1 - \sqrt{\frac{\sum_{i=k}^{k+T_h} [F_{exc}(i) - \hat{F}_{exc}(i|i-1)]^2}{\sum_{i=k}^{k+T_h} F_{exc}(i)^2}} \right)}{(t_{end} - t_0)} \quad (2.58)$$

Here,  $T_h$  is the prediction horizon counted in number of steps, and  $t_0$  and  $t_{end}$  are the start and end step of the time series, respectively.

## 2.6 Estimation of Excitation Force

### 2.6.1 Kalman Filter

The estimation process is carried out by obtaining information regarding the signal of interest  $F_{exc}(t)$  to estimate  $\hat{F}_{exc}(t + \tau)$  at some time  $t + \tau$ . If  $\tau > 0$ , the filter is called **prediction** filter (previous chapter), if  $\tau < 0$ , it is **smoothing** filter, and finally if  $\tau = 0$ , it is **filtering** operation. [8]

#### 2.6.1.1 Kalman Filter Dynamical System

Identification of the dynamical system and its matrices plays a key role in implementing Kalman filter estimator. Hence, in this section dynamical system of model in form of state space equation and derivation of its matrices will be explained.

Considering dynamical system including Gaussian white noise as;

$$\hat{s}_{k+1} = A\hat{s}_k + Bu_k + Gw_k \quad (2.59)$$

$$y_k = H\hat{s}_k + v_k \quad (2.60)$$

$$w_k(0, Q) \quad (2.61)$$

$$v_k(0, R) \quad (2.62)$$

Where the  $\hat{s}_k$  is the system estimated states including position, velocity, excitation force, derivative of excitation force, and radiation model state vector.  $y_k$  is the measurements of the position and vertical velocity which usually is the data that can be obtained through sensors or from devices such as accelerometer. In this work this data is achieved from simulation result and the Gaussian white noise is added afterwards.

The dynamic of excitation force is modeled as superposition of finite number of harmonic oscillators with different frequencies and phases;

$$F_{exc} = F_{exc_1} + F_{exc_2} + \dots + F_{ex_n} = A \sum_{i=1}^n \cos(\omega_i t + \phi_i) \quad (2.63)$$

The  $w_k$  and  $v_k$  are the Gaussian white noise in the process and the measurement respectively, while  $Q$  and  $R$  are considered as the white noise covariance matrices of the process and measurement, respectively.  $Q$  and  $R$  matrices represent the values (trade-off) between the accuracy and excitation force's noise level, which are symmetric positive and semi-definite matrices and are defined accordingly. Knowing definition of white noise vector i.e. a random vector of real number by probability distribution, with zero mean, and finite variance which are statistically independent. Or in the other words, two variables are statistically uncorrelated with zero covariance. Therefore, covariance matrix of white noise vector must be  $n$  by  $n$  diagonal matrix in which the diagonal elements are variances of components. [11]

And finally,  $A$  is the dynamical system matrix,  $H$  is the measurement matrix,  $G$  is weighting matrix for the state error, since there is no control input in this system, therefore, second term of the equation will be omitted.

Back to dynamical system equation, in this work, one can numerically demonstrate these matrices in continuous time as follows;

$$\begin{bmatrix} \dot{S} \\ \ddot{S} \\ \dot{F}_{exc} \\ \ddot{F}_{exc} \\ \dot{z} \end{bmatrix} = \begin{bmatrix} 0 & 1 & 0 & 0 & 0 \\ C_S & C_{\dot{S}} & C_{F_{exc}} & 0 & C_r \\ 0 & 0 & 0 & I & 0 \\ 0 & 0 & -\Omega^2 & 0 & 0 \\ 0 & B_r & 0 & 0 & A_r \end{bmatrix} \begin{bmatrix} S \\ \dot{S} \\ F_{exc} \\ \dot{F}_{exc} \\ z \end{bmatrix} + B \times 0 + \begin{bmatrix} 0 & 0 & 0 & 0 & 0 \\ 0 & 0 & 0 & 0 & 0 \\ 0 & 0 & 1 & 0 & 0 \\ 0 & 0 & 0 & 1 & 0 \\ 0 & 0 & 0 & 0 & 0 \end{bmatrix} w_k \quad (2.64)$$

$$\begin{bmatrix} y \\ \dot{y} \end{bmatrix} = \begin{bmatrix} 1 & 0 & 0 & 0 & 0 \\ 0 & 1 & 0 & 0 & 0 \end{bmatrix} \begin{bmatrix} S \\ \dot{S} \\ F_{exc} \\ \dot{F}_{exc} \\ z \end{bmatrix} + v_k \quad (2.65)$$

Where  $C_S$  is coefficient corresponds to the position,  $C_{\dot{S}}$  is coefficient corresponds to velocity,  $C_{F_{exc}}$  is the coefficient corresponds to the excitation force,  $I$  is to the identity matrix, and  $\Omega$  is a diagonal matrix with the fixed frequencies.

$$\Omega = \begin{bmatrix} \omega_1 & 0 & 0 \\ 0 & \omega_2 & 0 \\ \vdots & \ddots & \vdots \\ 0 & 0 & \omega_i \end{bmatrix} \quad (2.66)$$

Considering changing the frequencies, meaning that the frequencies of the excitation force are changed by changing the time, the estimation problem becomes nonlinear and an EKF must be applied in this scenario. [2]

### 2.6.1.2 Kalman Filter Assumptions

The following assumptions should be taken into consideration; [8] for time varying approach that will be explained in the next section.

- In summary, as mentioned in Kalman Filter Dynamical System the process and measurement noise  $w_k$  and  $v_k$ , are uncorrelated, zero mean with known covariance matrices.
- Considering random uncorrelated vector,  $s_0$ , to both the system and measurement noise processes as an **initial system state**.
- Considering known mean and covariance matrix for initial system state.

$$\hat{s}_{0|0} = E[s_0] \quad (2.67)$$

and

$$P_{0|0} = E \left[ (\hat{s}_{0|0} - s_0)(\hat{s}_{0|0} - s_0)^T \right] \quad (2.68)$$

Knowing the above assumption and given a set of measurement  $y_1, \dots, y_{k+1}$ , the Kalman filter should yield an optimal estimate of the state  $s_{k+1}$  at time instant  $k + 1$  that minimize the squared error loss function as follows;[8]

$$E \left[ \|s_{k+1} - \hat{s}_{k+1}\|^2 \right] = E[(s_{k+1} - \hat{s}_{k+1})^T (s_{k+1} - \hat{s}_{k+1})] \quad (2.69)$$

### 2.6.1.3 Kalman Filter Process

#### 2.6.1.3.1 Time Varying Kalman Filter

The time varying KF process has two steps, one the prediction or time update (TU) and the other the correction and measurement-update (MU).

KF a priori (TU):

In this process, due to injection of uncertainty of process noise  $w_k$ , the covariance error increases.

$$P_{k+1}^- = AP_k A^T + GQG^T \quad (2.70)$$

$$\hat{s}_{k+1}^- = A\hat{s}_k \quad (2.71)$$

On which, the estimate variance  $P_{k+1|k}$  is the mean squared error in the estimate of  $\hat{s}_{k+1|k}$ .

KF a posteriori estimation (MU):

Here, the sensors provide the next real measurement. So, as a result, the covariance error is decreased by adding measurement information.

$$K_{k+1} = P_{k+1}^- H^T (HP_{k+1}^- H^T + R)^{-1} \quad (2.72)$$

$$P_{k+1} = (I - K_{k+1}H)P_{k+1}^- \quad (2.73)$$

$$\hat{s}_{k+1} = \hat{s}_{k+1}^- + K_{k+1}(y_{k+1} - H\hat{s}_{k+1}^-) \quad (2.74)$$

Here,  $K_{k+1}$  is the residual weighting coefficient that provides an optimal weighting between model and measurement. Moreover, the updating process, by assuming that the estimate is a linear weighted sum of the time update(prediction) and new observation can be done.

The Kalman Filter performance can be also shown in block diagram as Figure 9; [14]

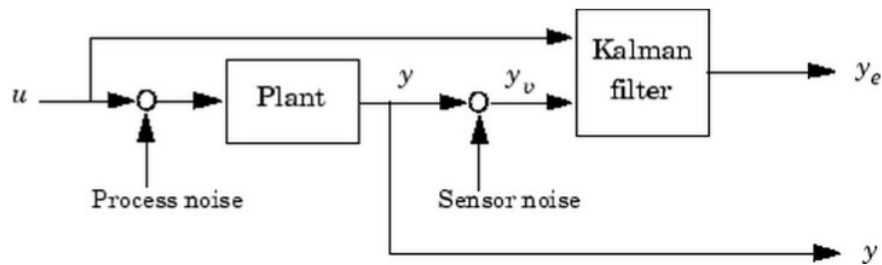


Figure 9 Kalman Filter block diagram.

Retrieved May 26, 2019 from <https://se.mathworks.com/help/control/ug/kalman-filtering.html>

Where  $y$  is the plant output states, and  $y_e$  is the estimated states from Kalman Filter.

### 2.6.1.3.2 Steady State Kalman Filter

The steady state Kalman Filter has the following equations;

- Measurement update;

$$\hat{s}_k = \hat{s}_k^- + M(y_k - C\hat{s}_k^-) \quad (2.75)$$

- Time update;

$$\hat{s}_{k+1}^- = A\hat{s}_k + Bu_k \quad (2.76)$$

In order to estimate the excitation force, time update acts as one step ahead predictor, to predict the state value of next sample (k+1). The adjusting of the estimation process is accomplished through measurement updates, based on the new measurements  $y_{k+1}$ . Further on, the correction process, i.e. discrepancy between measured and estimated value of  $y_{k+1}$  also called innovation, is performed through  $(y_k - C\hat{s}_k^-)$ .

Minimization of the steady-state covariance matrix of the process and the measurement noise is accomplished through the innovation gain  $M$ .

$$E(w_k w_k^T) = Q \quad E(v_k v_k^T) = R \quad N = E(w_k v_k^T) = 0 \quad (2.77)$$

By combining the time and measurement updates, the steady-state Kalman Filter can be described as one state-space model as follows;

$$\hat{s}_{k+1}^- = A(I - MC)\hat{s}_k^- + [B \ AM] \begin{bmatrix} u_k \\ y_k \end{bmatrix} \quad (2.78)$$

$$y_k = C(I - MC)\hat{s}_k^- + CM y_k \quad (2.79)$$

## 3 METHODS

### 3.1 Information Flow from Measurement to Predicted Signal

The following block diagram shows the schematic of the system model and the information flow from measurement to predicted signal.

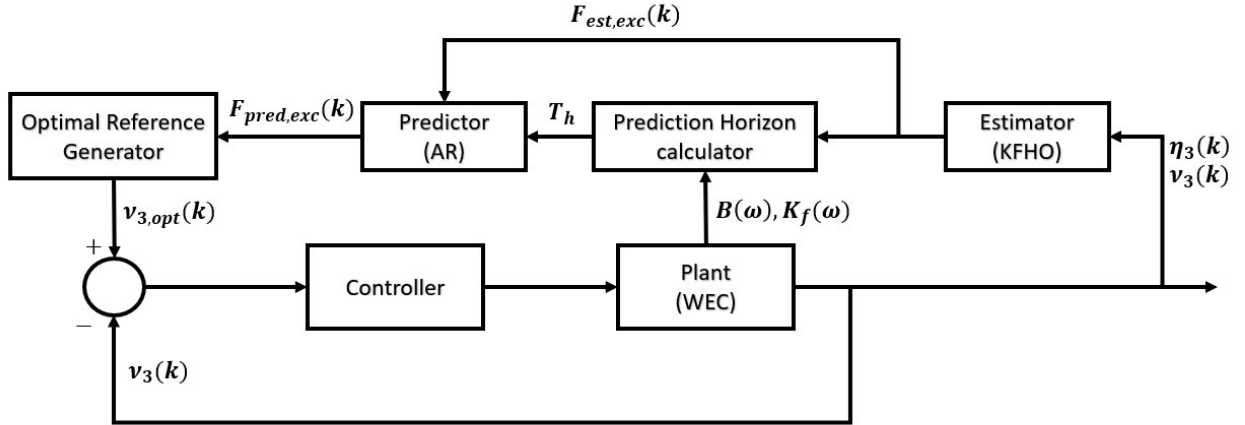


Figure 10 The block diagram representing the information flow from measurement to prediction

The tool used in this work for performing calculations is MATLAB 2016.

### 3.2 WEC Model

The CPO WEC model parameters that is used in each section of this work is summarized in Table 2 with the following specification and assumption:

- Hydrodynamical parameters are calculated by the software WAMIT.
- Assumption of movement of the device only in heave direction out of six degree of freedom has been considered for the sake of simplification.

Table 2 Parameters of CPO WEC model used for this study.

	Prediction Horizon, Prediction of Excitation Force, and Estimation of Excitation Force
$A_{wp}^{(1)}$	81.6745 m <sup>2</sup>
$V_{eq}^{(2)}$	284.55 m <sup>3</sup>
$m_b^{(3)}$	22000 kg

(1) Water plane area

(2) Volume of the WEC in the equilibrium position

(3) Mass of the WEC

For calculation of prediction horizon and prediction of excitation force, data set corresponds to 30 minutes has been used, while in estimation of excitation force, data set for 2 minutes is considered. Finally, for calculation of the combination of prediction and estimation of excitation force, data set for 23 min is taken.

### 3.3 Prediction Horizon

In order to calculate the optimal velocity as a function of prediction horizon, first the transfer function ( $H_{opt}$ ) is derived in frequency domain knowing the radiation resistance and of the system. Figure 11 and Figure 12 show the radiation resistance and the transfer function in frequency domain.

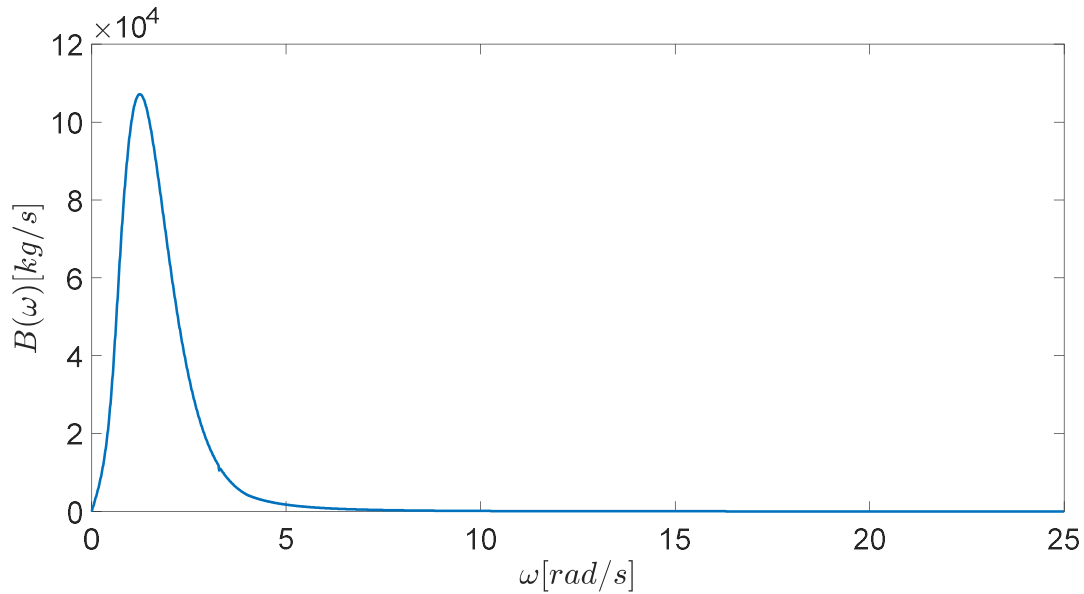


Figure 11 Radiation Resistance vs frequency

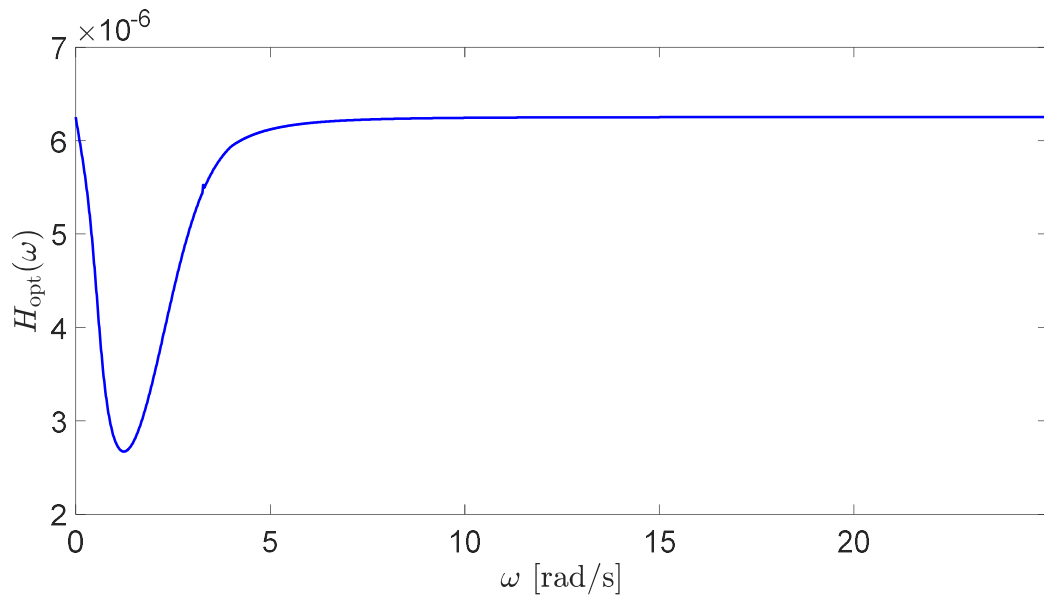


Figure 12 Noncausal transfer function between excitation force and optimal velocity, i.e. even and real function of the frequency

To reduce the computational complexity of the prediction horizon,  $H_{opt}(\omega)$  is filtered and only its attenuation band is considered. This assumption is valid due to the following reasons: [3]

- The frequency content of the excitation force is usually within the stopband of  $H_{opt}(\omega)$
- In real sea states, waves do not appear at frequencies below 0.2-0.3 rad/s

As a result, the noncausality of optimal velocity will be reduced while it still has significant influence in all sea states. Figure 14 shows the filtered transfer function based on dominant frequency contents of excitation force.

It is therefore assumed that the distribution of excitation force is well known for the whole frequency range, as it is illustrated in Figure 13. The sea state by 1.8m significant wave height and peak period of 12.5s is taken for the purpose of the analysis.

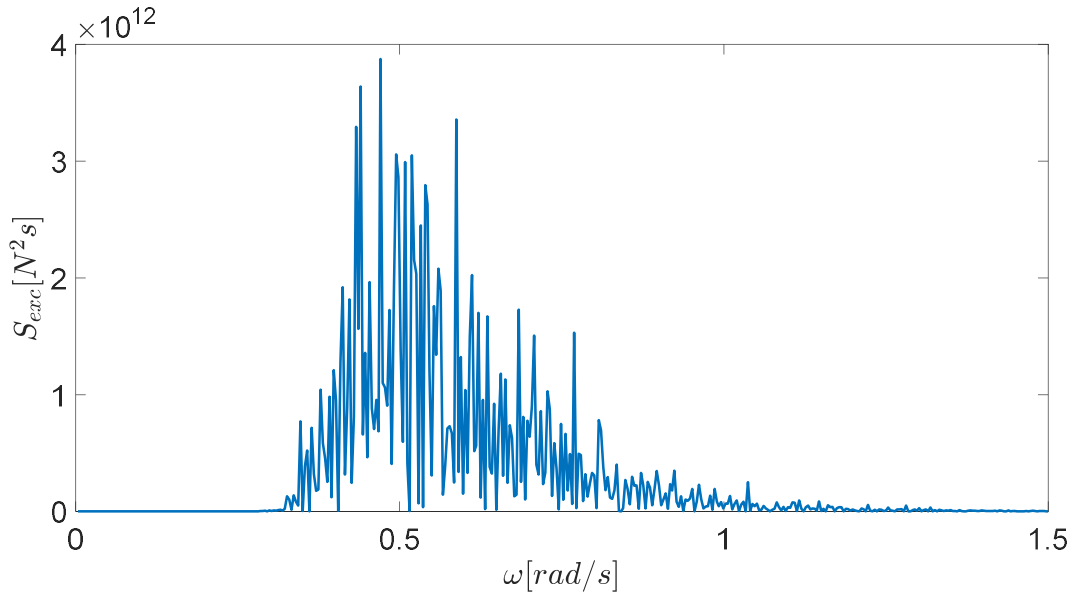


Figure 13 Spectral density of the excitation force for sea state with 1.8m significant wave height and peak period of 12.5s

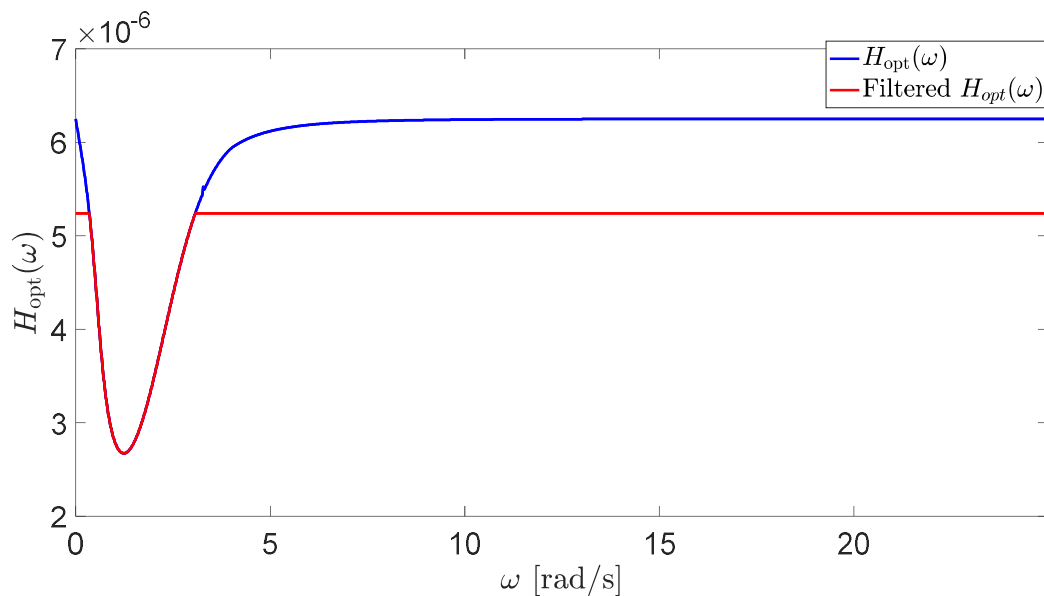


Figure 14 Comparing filtered and non-filtered transfer function between excitation force and optimal velocity

Since the transfer function  $H_{opt}(\omega)$  yields to a constant value when  $\omega \rightarrow \infty$ ,  $k_{opt}(\omega)$  is computed. As a result, the inverse Fourier transform of  $K_{opt}(\omega)$  is now well defined. Figure 15 shows the filtered and nonfiltered of  $K_{opt}$  in frequency domain.

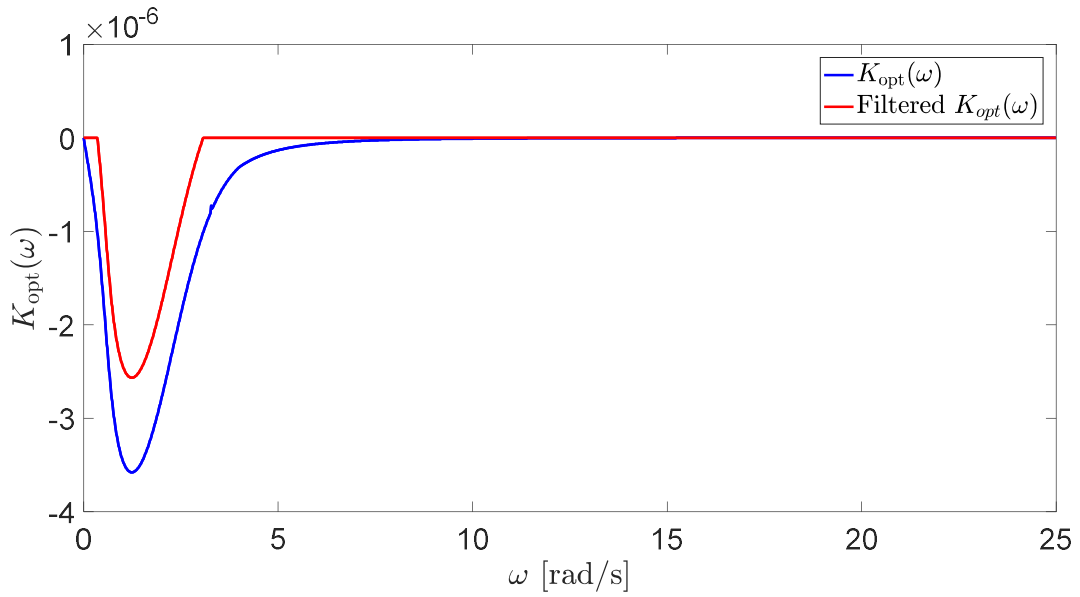


Figure 15 Transfer function  $K_{opt}(\omega)$  in frequency domain

Impulse response function  $k_{opt}(t)$  is then computed with the aid of fast Fourier inverse function in MATLAB. Figure 16 illustrate the filtered and nonfiltered of  $k_{opt}$  in time domain and its evenness.

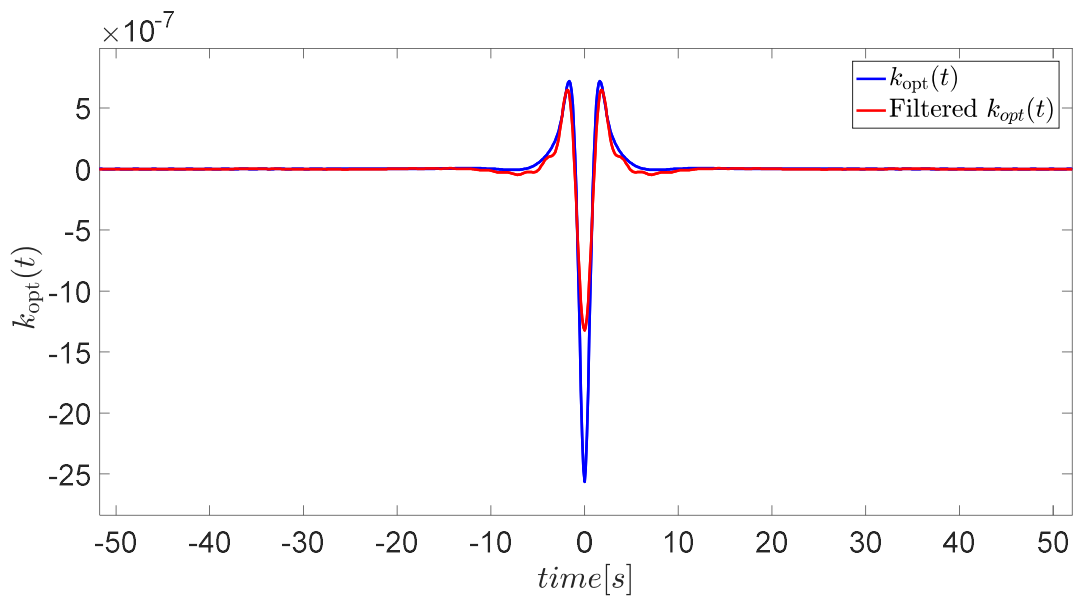


Figure 16 Impulse response  $k_{opt}(t)$  in time domain

Now, the required functions are determined in time domain. The suboptimal oscillation velocity is introduced as a truncated integral. The evenness of impulse response has been maintained by also truncating the causal part of the integral.

This calculation requires the knowledge of future values of excitation force. In this work, it is assumed that these values are perfectly known for any time horizon.

$$v_{opt}^{T_h}(t) = \int_{-T_h}^{T_h} h_{opt}(t) f_{exc}(t - \tau) d\tau \quad (3.1)$$

Hence the suboptimal velocity is derived as a function of prediction horizon. Assuming that the suboptimal velocity is equal to the optimal velocity for the maximum available horizon, i.e. derived from the maximum available corresponding time of  $k_{opt}(t)$ .

In order to estimate the error of the computed suboptimal velocity, GoF (Goodness-of-fit) is used;

$$GoF = 1 - \sqrt{\frac{\sum (v_{opt} - v_{opt}^{T_h})^2}{\sum v_{opt}^2}} \quad (3.2)$$

### 3.4 Prediction of Excitation Force

In order to predict the excitation force with an AR model, the following assumptions have been considered in this work.

- To assess the performance of the AR model, the synthesized excitation force spectrum is assumed to be well-known to provide a comparison between the synthesized and predicted excitation force.
- Low pass filter has been used to remove high frequency content in excitation force spectrum to improve the performance of the prediction.
- The regression coefficient matrix  $\phi^*$  is presumed to be constant during the whole prediction horizon.

#### 3.4.1 Filtering the excitation force

The high frequency content of excitation force is out of interest due to containing a low level of energy, therefore, a low pass filter has been applied which resulted in improvement of the predictability of the wave data while considering only low frequency component in which excitation force has high act energy content. Note the cut off frequency is chosen according to the visual inspection of the spectral shape of each data set. The choice of cut off frequency can play an important role in prediction of future data by compromising the prediction accuracy and amount of the discarded components of energy. [24]

The low pass filter with cut off frequency of 1.26 Hz is applied the effect of which is illustrated in frequency and time domain in Figure 17 and Figure 18.

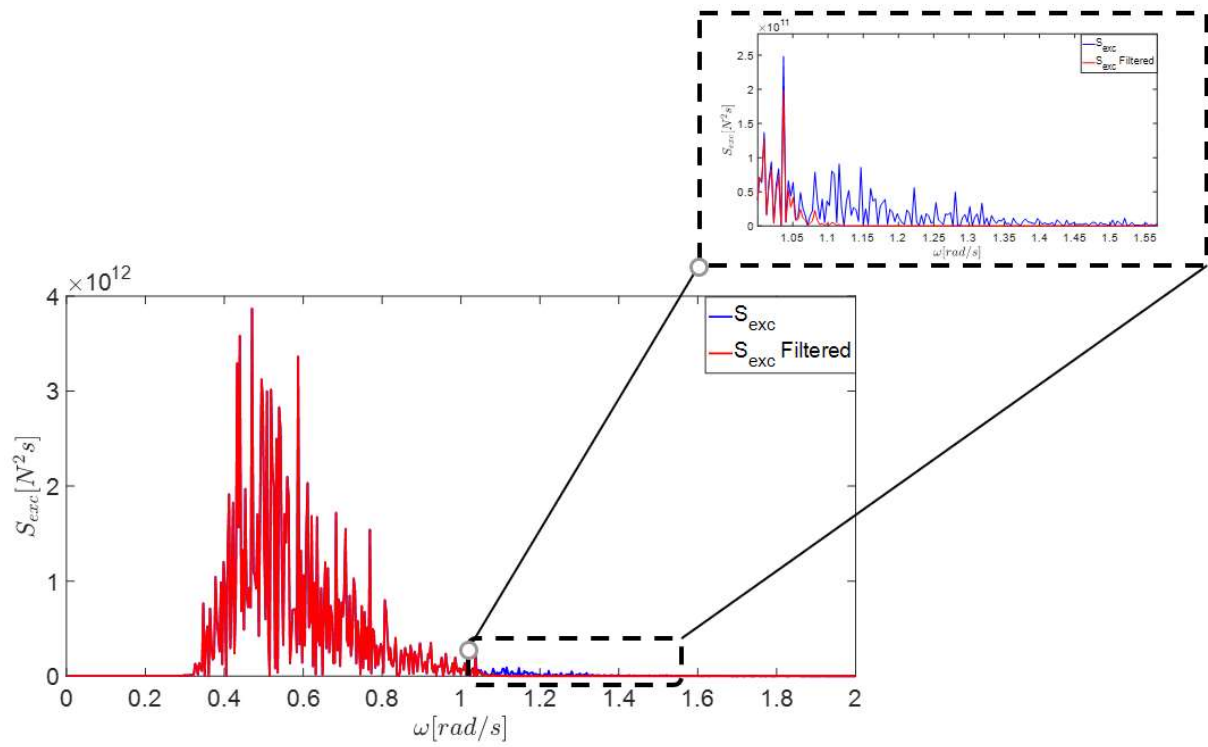


Figure 17 Filtered and unfiltered excitation force spectral density

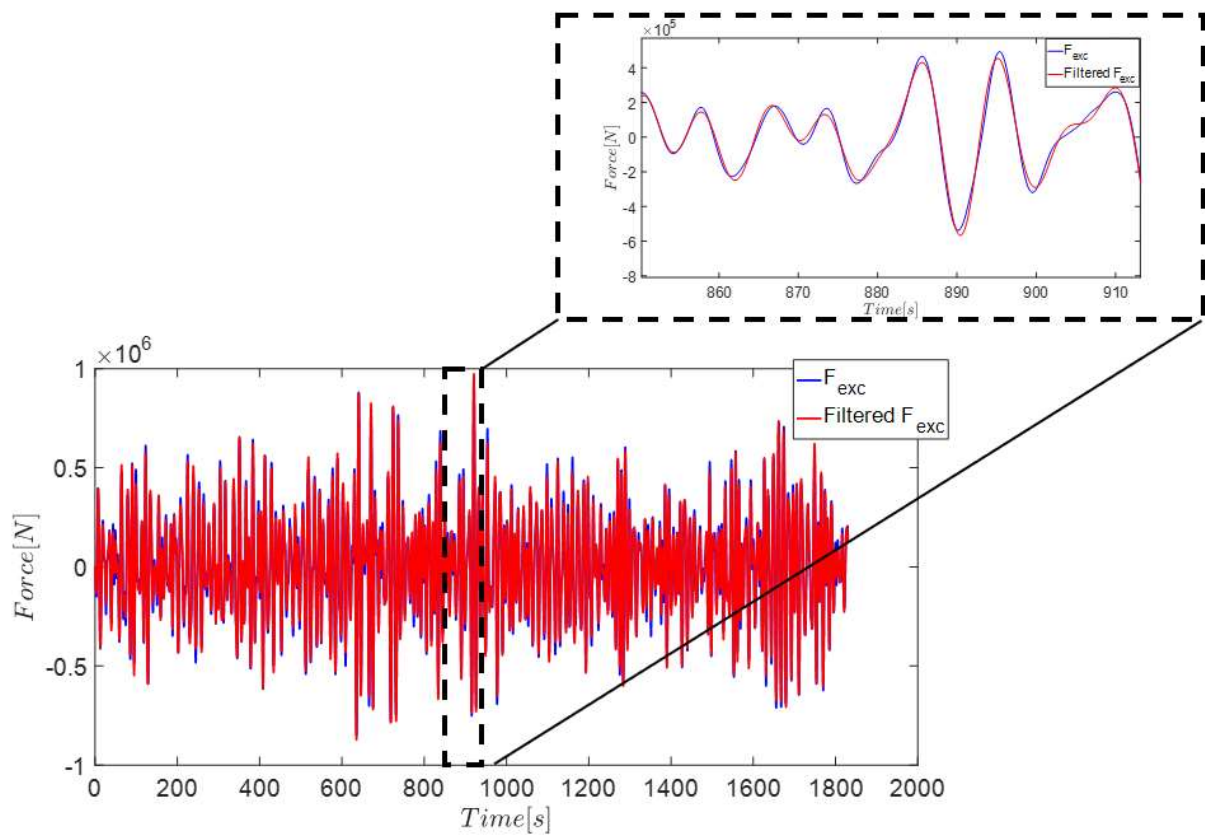


Figure 18 Filtered and unfiltered excitation force in time domain.

### 3.4.2 Coherence Time

The autocorrelation function of a time series signal is the correlation of a signal with a delayed copy of itself. If the autocorrelation function is above a certain threshold, it means that the signal can be approximated by its sinusoidal extrapolation. The corresponding time for this threshold is called the coherence time,  $\tau_c$ . Informally, for delay values below the coherence time, there is similarity between the delayed copy of the signal and the signal itself.

Following this explanation, the model order of the predictor times its sampling time should always be lower than the coherence time,  $p \leq \tau_c$ . This can provide a range limit to find the optimum model order. Figure 19 shows the autocorrelation function of the excitation force over time. It can be seen that the coherence time is about 30s.

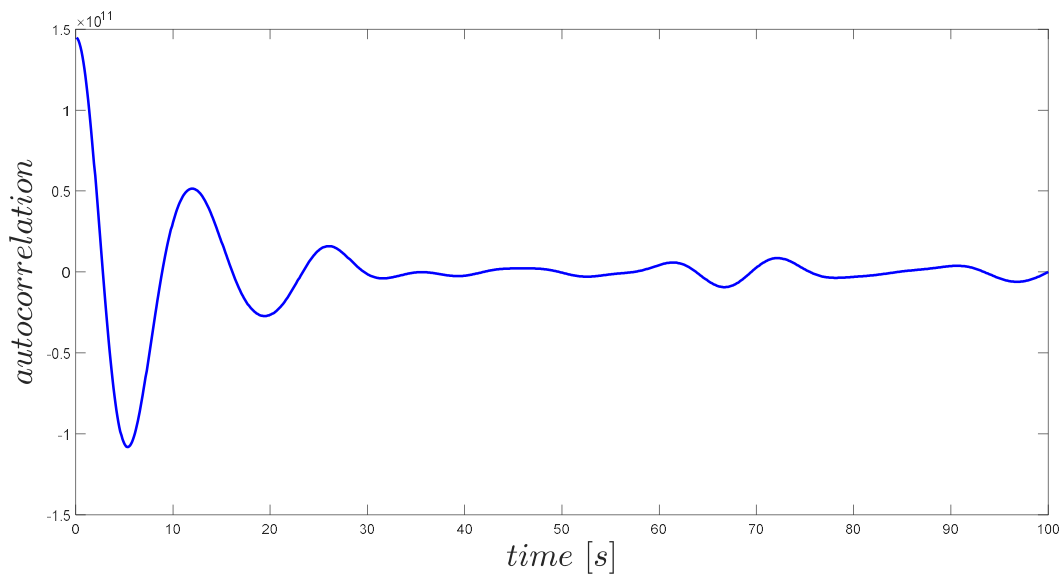


Figure 19 Autocorrelation function of excitation force vs time

### 3.4.3 AR Optimization

Changing the AR parameters such as  $N$ , and  $p$  will affect the predictor performance. As a result, the optimization is essential to derive the best model parameters based on the predefined success criteria (GoF).

In this section, the optimization is performed by varying the model parameters in several steps. In all steps, the starting time instance of the prediction is set as 70s, and the sampling time of  $F_{exc}$  as 0.1s. The GoF is calculated for all time instances and the average value is reported in all optimization steps.

In the first step, the prediction horizon is fixed at 5s according to the Prediction Horizon section which is a reasonable value for the start due to comparable high Goodness-of-fit for optimal velocity. Then the GoF for the excitation force prediction is plotted versus  $N$  and for various model orders ( $p$ ).

In the second step, an optimal value of  $N$  has been chosen with the same prediction horizon from the first step, and then the GoF is plotted for different model order numbers to find the optimal  $p$  value.

In the third step, the GoF is displayed as a function of prediction horizon for different  $p$  values to assure the foremost prediction horizon and  $p$  values.

In the last step, the tuned  $p$  and  $N$  values from previous steps have been set constant, and it is found interesting to check the accuracy of the prediction model for different sampling times when the excitation force is resampled at different frequencies.

Finally, considering the optimum parameters of the AR model, the N-step-ahead prediction is calculated and compared with the measured excitation force. In N-step-ahead prediction, at each time step only the last predicted point of the horizon is considered.

It means that assuming standing at time  $t_0$ , the AR predicts the excitation force for the time period of  $t_0$  to  $t_0 + T_h$ , then the prediction for the last point ( $t = t_0 + T_h$ ) is saved. Continuing saving all these points for the entire time series gives the N-step-ahead prediction of the excitation force.

The GoF of this prediction is calculated as the GoF for all N-step-ahead predicted points.

### 3.4.4 Numerical Computation of AR Coefficients

As stated in the assumption, the AR coefficients are kept constant and in order to compute the corresponding matrix of the regression coefficients, the *symmlq* method has been used that provides an iterative method with a specified tolerance for solving the linear system of equations.

## 3.5 Estimation of Excitation Force

One of the challenges in establishing an estimator for excitation force, is to linearize the forces of the system to be used in state-space model of Kalman Filter.

The main purpose of linearization of the forces is to be able to model the system as mass-spring-damper system. Hence, the choice of applying Taylor expansion or equivalent viscous damping for the purpose of linearization depends on the characteristic of each force. With reference to Equation of Motion in Time Domain, the nonlinear forces are linearized according to following section.

### 3.5.1 Linearization of Non-Linear Forces

As it is shown in the equation of motion, drag and machinery forces introduce nonlinearity into the system. Two approaches have been used to linearize these forces.

- Linearization of spring forces by taking first order of Tylor expansion around the point of interest.
- Using equivalent viscous damping for linearization of damping forces [10]. This method provides accurate result along whole time series, and is explained briefly bellow;

If linear damping force is defined as;

$$F_{lin} = R_d v_{buoy} \quad (3.3)$$

Then, one can assume;

$$\int_{t_1}^{t_{end}} F_{NonLin} dt = \int_{t_1}^{t_{end}} F_{lin} v_{buo} dt \quad (3.4)$$

From above equation  $R_d$  can be derived and following that  $F_{lin}$  will be computed.

Following sections introduce the nonlinear forces and its linearization. The numbers on axis of the plots is removed due to the confidentiality reasons.

### 3.5.1.1 Drag Force

Non-linear drag force is function of the relative velocity between buoy and water velocity as is displayed as;

$$F_{D,NonLin} = -\frac{1}{2} A_3 C_{D3} \rho (v_3 - \xi_3) |v_3 - \xi_3| \quad (3.5)$$

By knowing that often buoy velocity is greater than water velocity, non-linear drag force is assumed as;

$$F_{D,NonLin} = -\frac{1}{2} A_3 C_{D3} \rho (v_3)^2 |v_3|^2 \quad (3.6)$$

By presuming mentioned assumption for non-linear drag force and using equivalent viscous damping, i.e. explained in [10], the linear force can be interpolated as;

$$E_{D,NonLin} = -\frac{1}{2} A_3 C_{D3} \int_{t_1}^{t_{end}} (v_3)^3 |v_3|^2 dt \quad (3.7)$$

$$F_{D,Lin} = R_{D,Lin} v_3 \quad (3.8)$$

Where  $E_{D,NonLin}$  corresponds to drag energy and  $R_{D,Lin}$  is drag damping.

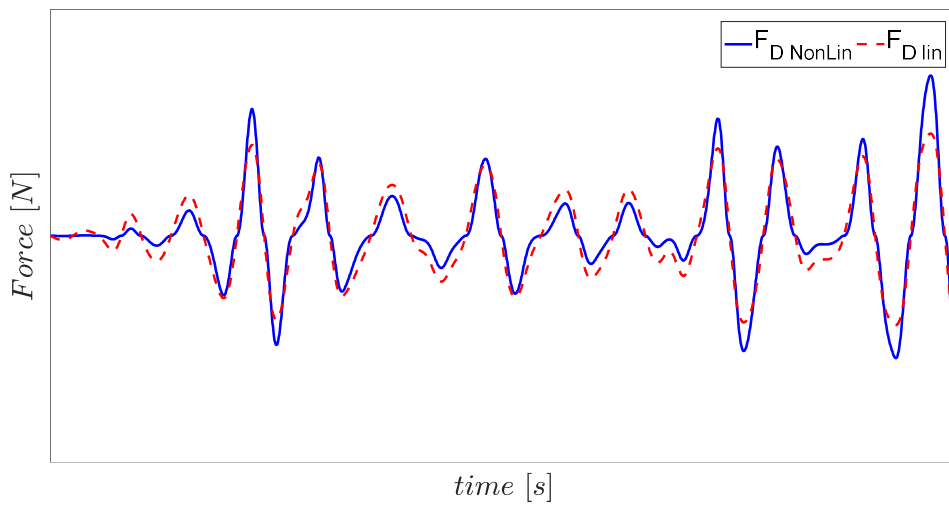


Figure 20 Linear drag force in blue compare to nonlinear drag force in red

As illustrated in Figure 20, there is a discrepancy between red and blue line that is due to non-linearity of the drag force.

### 3.5.1.2 Machinery Force

- Pretension Force

Considering the non-linear pretension force as is presented in the theory section, a linearized pretension force can be expressed as;

$$F_{p,Nonlin} = -(p_p - p_{atm})A_p - C_{v,p}v_3 \quad (3.9)$$

The non-linear pretension force can be divided in two terms. A loss term,  $-C_{v,p}v_3$ , can be taken as linear damper term; all the rest,  $-(p_p - p_{atm})A_p$ , can be considered as spring term and Taylor expansion around zero position can be applied to linearize this term.

The linear damper term of pretension force is hence;

$$F_{p,DLin} = -C_{v,p}v_3 \quad (3.10)$$

Linearization of the spring term by Taylor expansion;

$$F_{p,SNonLin} = -(p_p - p_{atm})A_p \quad (3.11)$$

$$K_{p,S} = \frac{dF_{p,SNonLin}}{d\eta_3} (0) \quad (3.12)$$

$$F_{p,SLin} = F_{p,SNonLin}(0) + K_{p,S}v_3 \quad (3.13)$$

Where  $F_{p,SNonLin}$  is the nonlinear spring term of pretension force,  $K_{p,S}$  is the spring stiffness of the pretension force, and  $F_{p,SLin}$  is the linear spring term of pretension force.

Then, the linear pretension force can be expressed as;

$$F_{p,Lin} = F_{p,DLin} + F_{p,SLin} \quad (3.14)$$

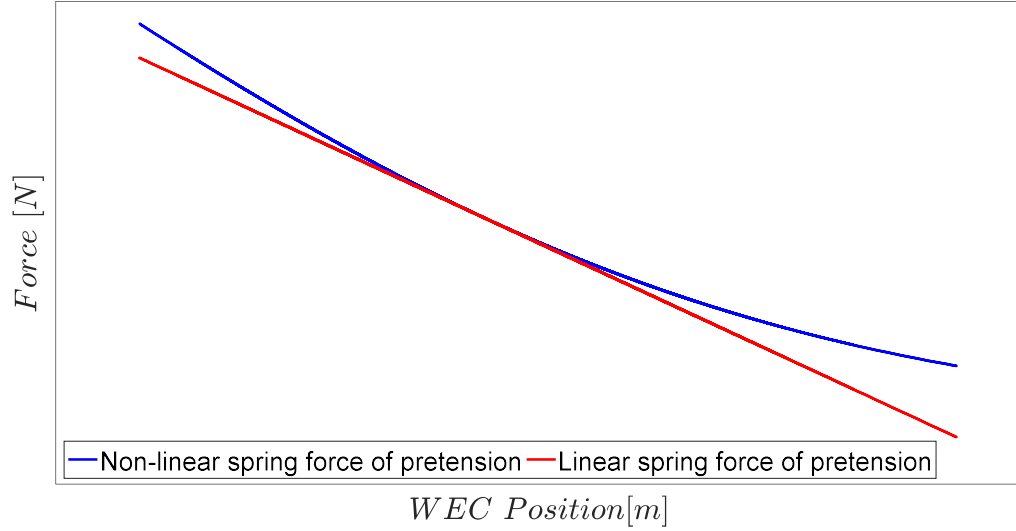


Figure 21 Non-linear spring terms of pretension force in blue versus linear spring term of pretension force in red

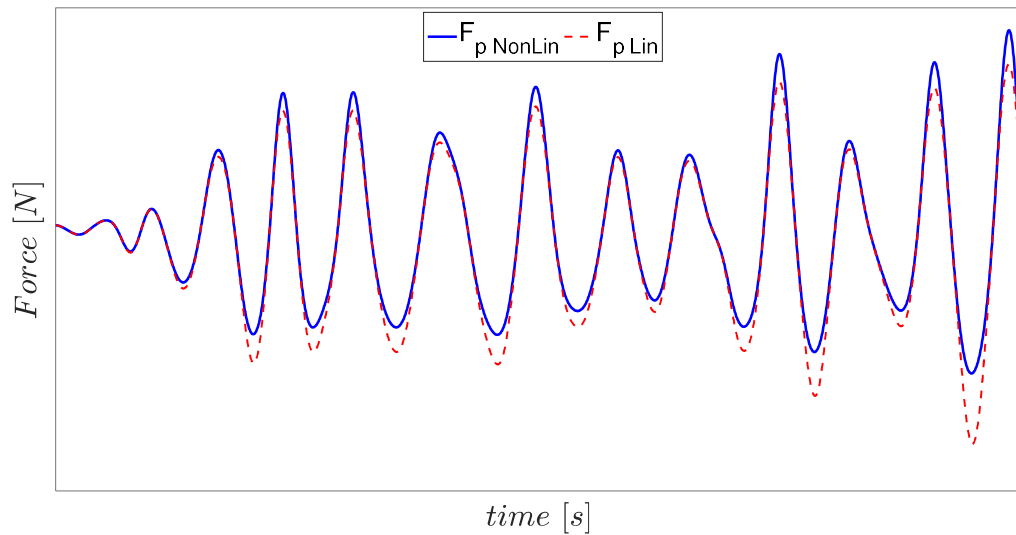


Figure 22 Non-linear pretension force in blue compare to linear pretension force in red

As it is demonstrated in Figure 22, the linear pretension force follows the non-linear pretension force with small discrepancy in term of its amplitude, since non-linear pretension force behaves fairly close to linear force as it is shown in Figure 21.

- WaveSpring Force

As it is depicted in theory section of Estimation of Excitation Force, non-linear wave spring force is;

$$F_{WS,SNonLin} = N_{WS} T_{r2W} (p_{WS} - p_{atm}) A_{WS} \quad (3.15)$$

Therefore, the WaveSpring force is only a nonlinear spring which can be linearized using Taylor expansion similar to the method in pretension force;

$$K_{WS,S} = \frac{dF_{WS,SNonLin}}{d\eta_3} (0) \quad (3.16)$$

$$F_{WS,Lin} = F_{WS,SNonLin}(0) + K_{WS,S}\nu_3 \quad (3.17)$$

Where,  $F_{WS,SNonLin}$  is the nonlinear spring term of WaveSpring force, and  $K_{WS,S}$  is the spring stiffness of the WaveSpring force. Figure 23 illustrates the comparison of the nonlinear and linear spring force term of the WaveSpring.

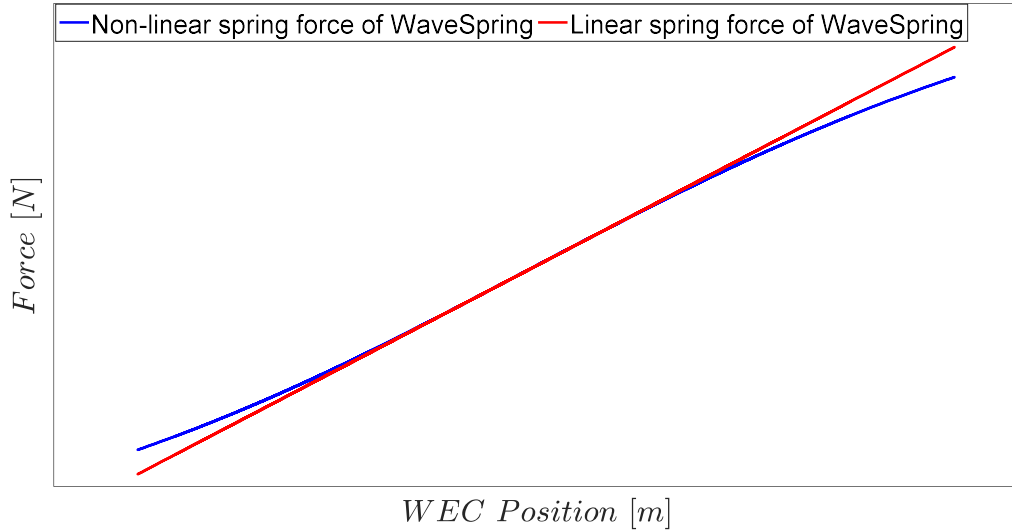


Figure 23 Linear spring force of WaveSpring in red and nonlinear spring force of the WaveSpring in blue.

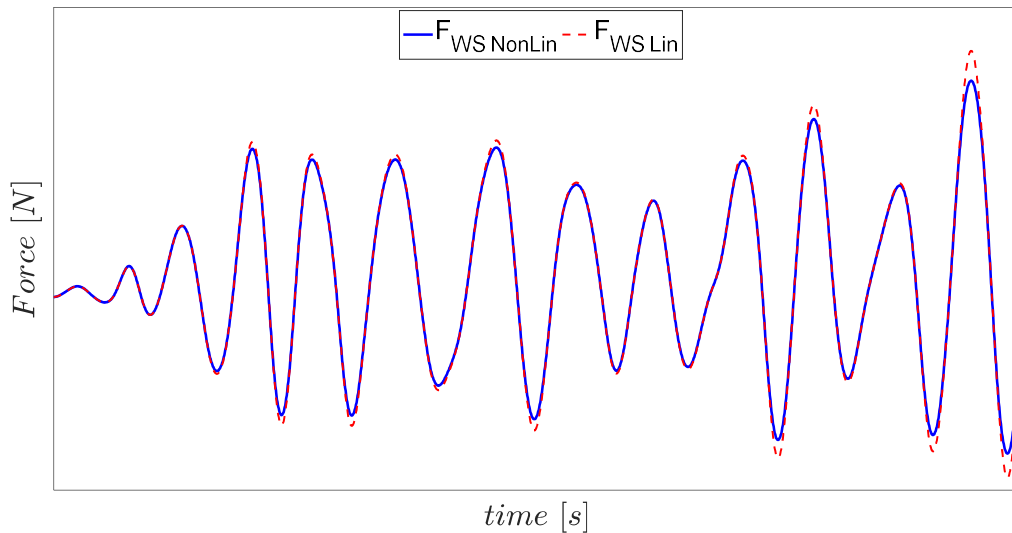


Figure 24 Nonlinear WaveSpring force in blue compare to linear WaveSpring force in red.

As it is shown in Figure 24, the linear WaveSpring force follows nonlinear force with small discrepancy in terms of amplitude at some time instance.

- Force corresponds to Mechanical Generator Loss

The last non-linear term in the equation of motion can be described as;

$$F_{MGL} = T_{gb}(\tau_{gen} + \tau_{l,mech}) \quad (3.18)$$

So, the linear force can be defined as written below by using equivalent viscous damping;

$$F_{MGL,lin} = R_{MGL,lin}v_3 \quad (3.19)$$

Where,  $R_{MGL,lin}$  is linear damping of the mechanical generator loss.

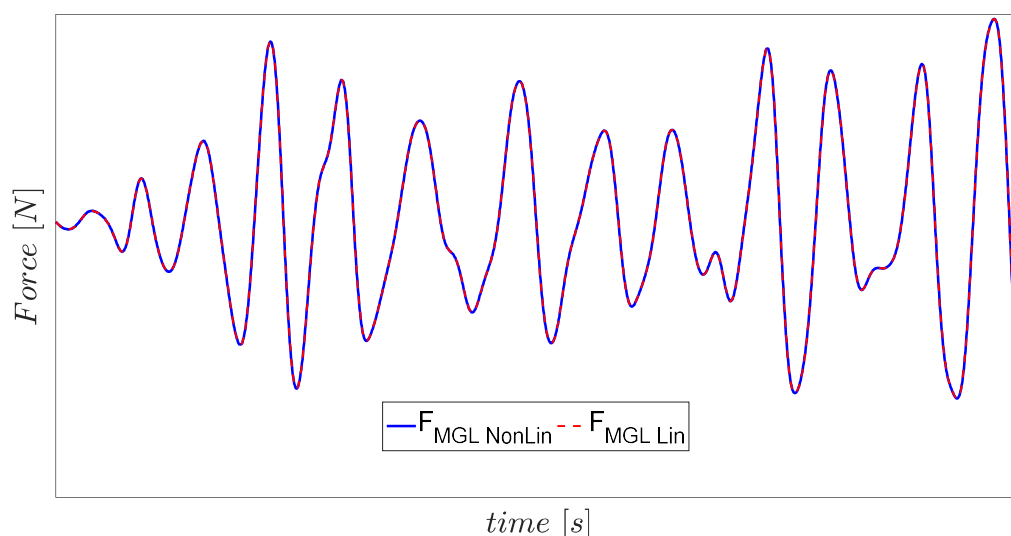


Figure 25 Comparison between linear and non-linear forces correspond to mechanical generator loss

Figure 25 illustrates that during entire time linear force in red follows nonlinear force in blue, i.e. shown that the nonlinear mechanical generator loss has fairly linear behavior.

### 3.5.2 Validation of linear system

As it is expressed, the nonlinear equation of motion by two linearization approaches is converted to linear to build up the state space equations of the Kalman filter based on linear equation of motion, and as a result, it introduces the linear system for Kalman filter.

In the end, the validity of the linearization is confirmed through the comparison of the response of the linear system with nonlinear system by taking the synthesized excitation force as an input for the both nonlinear and linear system, which has proved that the linear system produces fairly close response to nonlinear system for both position and the velocity as it is shown in Figure 26 and Figure 27.

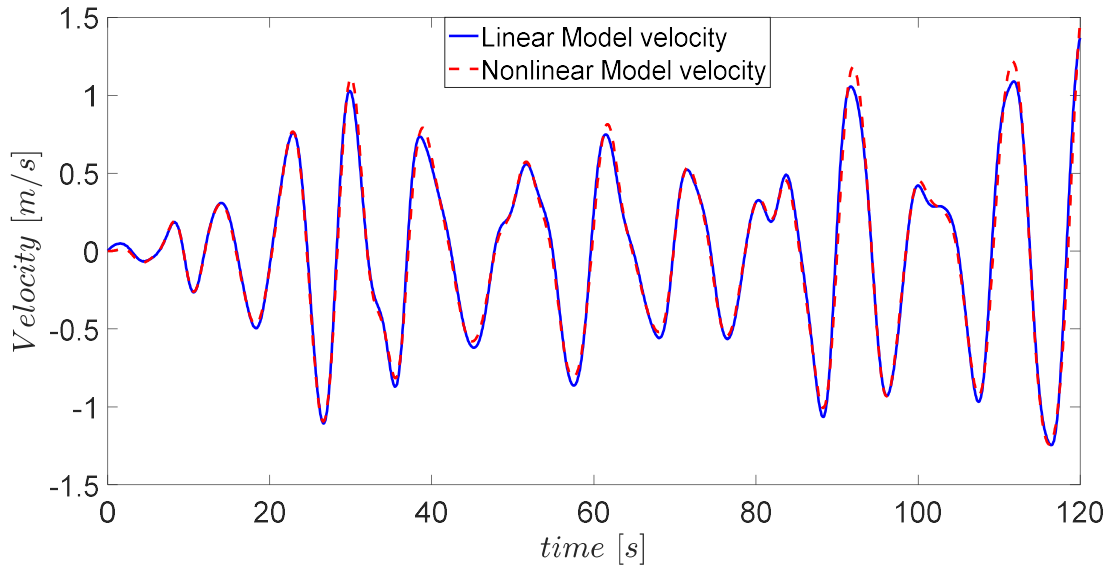


Figure 26 comparing WEC velocity for linear system model and nonlinear system model.

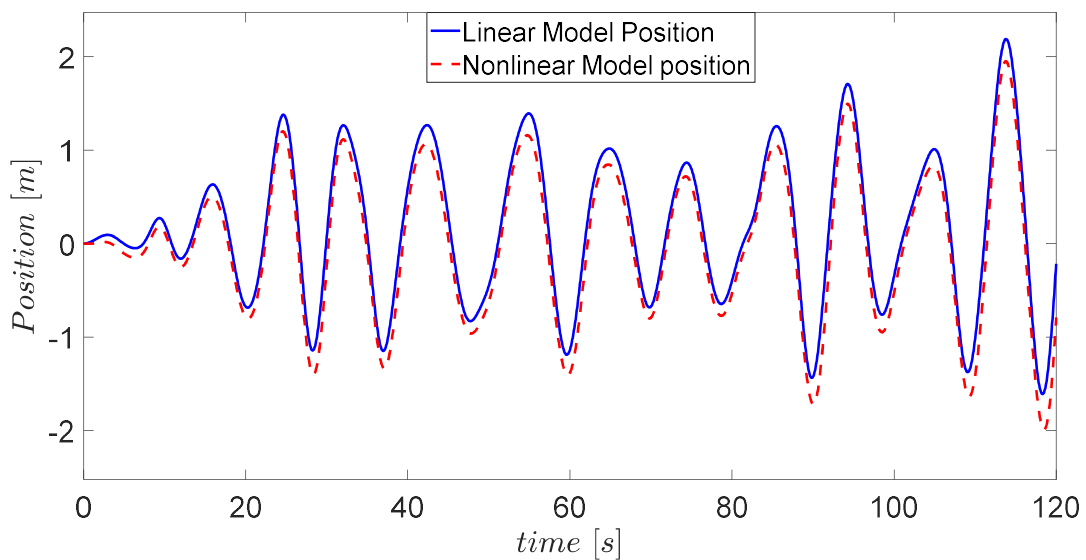


Figure 27 Comparing position of WEC for linear system model and nonlinear system model.

### 3.5.3 Kalman Filter Approaches

In the real case scenario, the input measurement vector to the Kalman filter with harmonic oscillator is taken from position and velocity sensors. While, in this case, the measurements are taken from simulation results of nonlinear plant system. However, to check the effect of the input vector to the Kalman Filter, the measurements derived from the linear plant response are also given as input vector to the estimator.

Both time varying and steady-state approaches are taken into consideration to check the validity of the estimation of the Kalman Filter with harmonic oscillator. The accuracy of these two methods is then compared.

### **3.6 Combining Prediction and Estimation of Excitation Force**

As the final step, the previously mentioned methods are combined together to verify the accuracy of the estimation to prediction process. So, first, KFHO estimates the excitation force and then AR model predicts the excitation force for the required prediction horizon. The AR model parameters have been adjusted for the estimated excitation force derived from Kalman Filter output in the last section, and finally the overall accuracy of the combined estimation and prediction is calculated by comparing the synthesized excitation force (derived from the nonlinear plant) and the predicted force from AR model.

It is assumed a different synthesized sea state from one that was used in prediction section to check validity of the methods for different excitation force data in different sea states.

## 4 RESULTS

---

### 4.1 Prediction Horizon

Figure 28 shows the Goodness-of-fit (GoF) for different prediction horizons. Increasing the prediction horizon improves the GoF, when eventually the optimal velocity will be achieved for  $T_h \rightarrow \infty$ .

Theoretically speaking, when  $T_h = 0$ , the noncausality in integration of suboptimal velocity is removed and no future values of excitation force is required which results in the lowest GoF.

In general, increasing the prediction horizon will result in better GoF, however this trend is identified according to the impulse response function and the excitation force in a specified sea state.

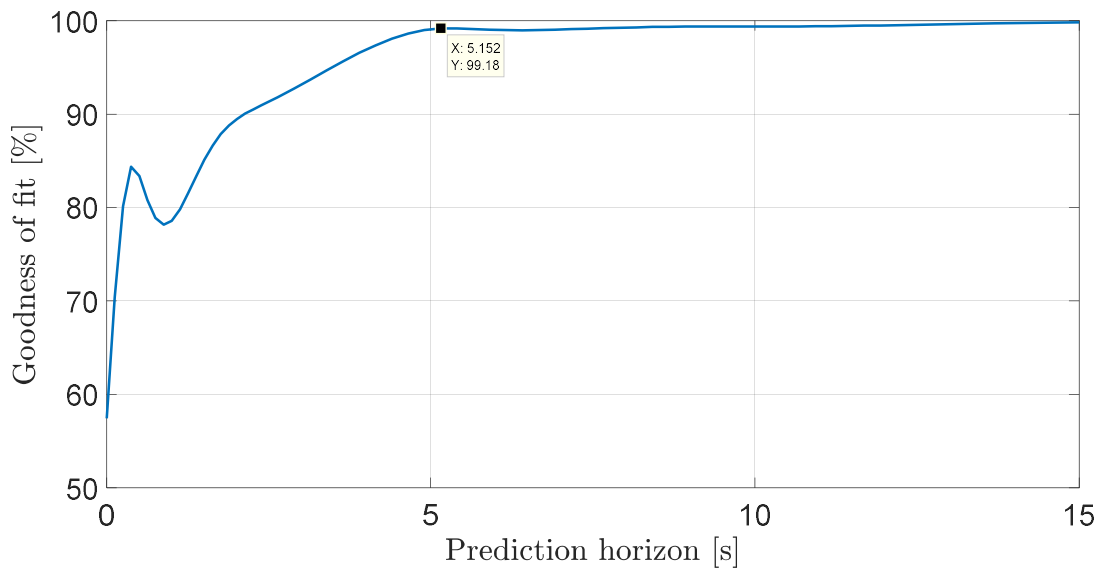


Figure 28 Goodness of Fit vs Prediction Horizon

### 4.2 Prediction of Excitation Force

First the AR optimization curves are presented and then the model with optimal parameters is applied to predict the excitation force within the specified horizon. In all the steps,

#### Step 1:

In Figure 29, the GoF has been plotted as a function of the number of trained values. Overall, for all model orders, the increase in  $N$  results in better prediction accuracy. According to this figure the optimal model order and training value have been selected.

#### Step 2:

The AR model is applied for different horizons in Figure 30, and it is evident that the error will increase for all AR orders by increasing the horizon.

**Step 3:**

In Figure 31, the performance of the predictor is shown as a function of sampling time for various prediction horizons.

Lastly, following several optimizations steps the optimal predictor parameter is determined. In Figure 32, N-step-ahead predicted excitation force comparing to measured excitation force is displayed. Table 3 shows the GOF of AR predictor compared to the measured and filtered excitation force for N-step-ahead-prediction.

Table 3 GoF for N-step-ahead prediction by AR predictor.

GoF	Predicted compared to measured excitation force	Predicted compared to filtered excitation force
$Th = 5s$	88.6%	99.1%

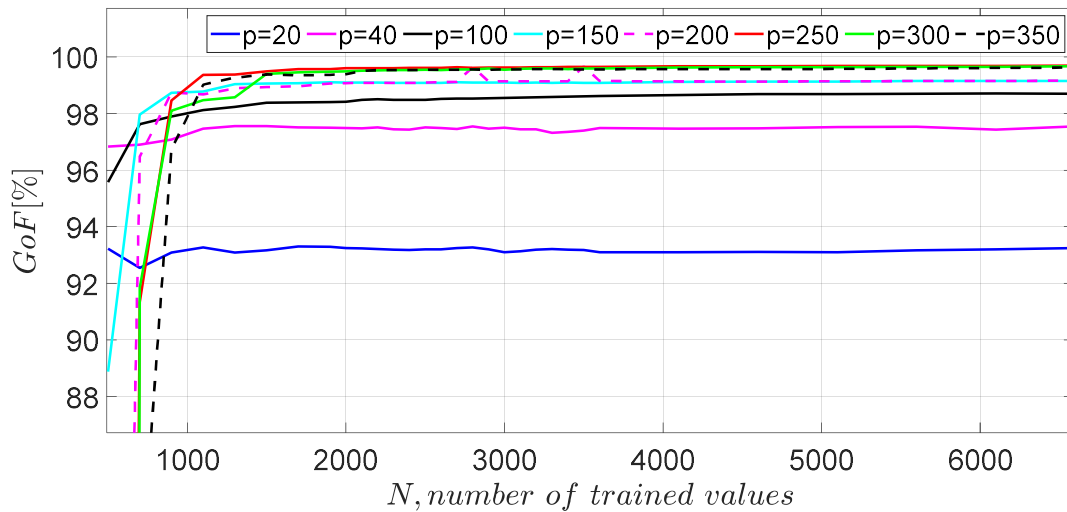


Figure 29 Optimization Step 1; GoF vs N number of trained values for different model orders

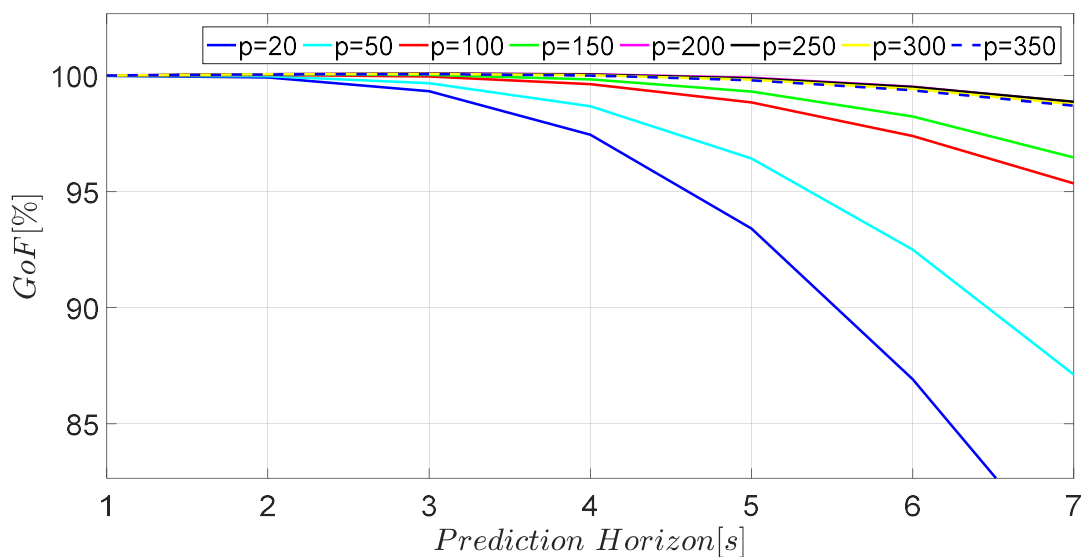


Figure 30 Optimization Step 3; GoF vs Prediction Horizon for different model orders with  $N = 3500$

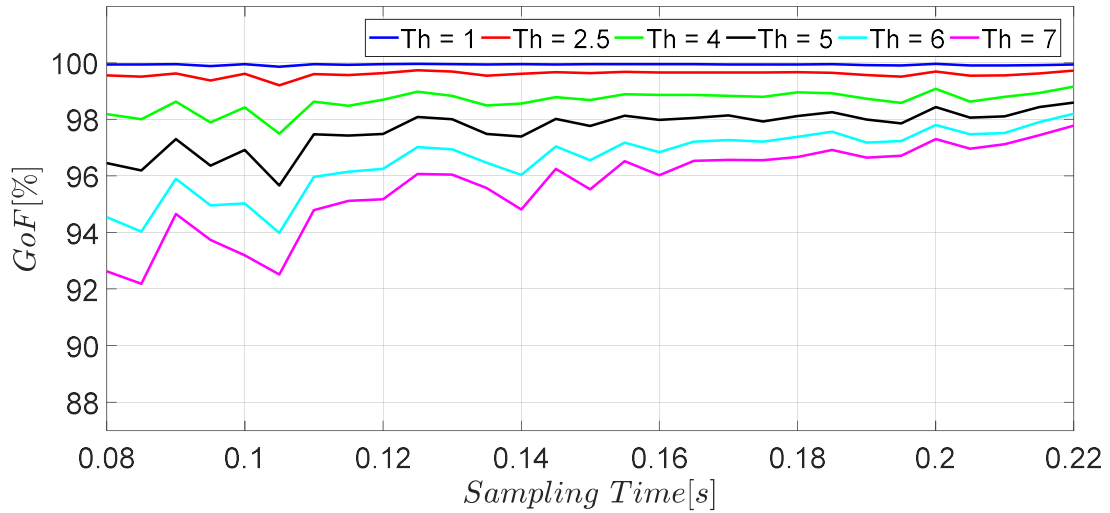


Figure 31 Optimization Step 4; GoF as a function of sampling frequency for different prediction horizons,  $p = 250, N = 3500$

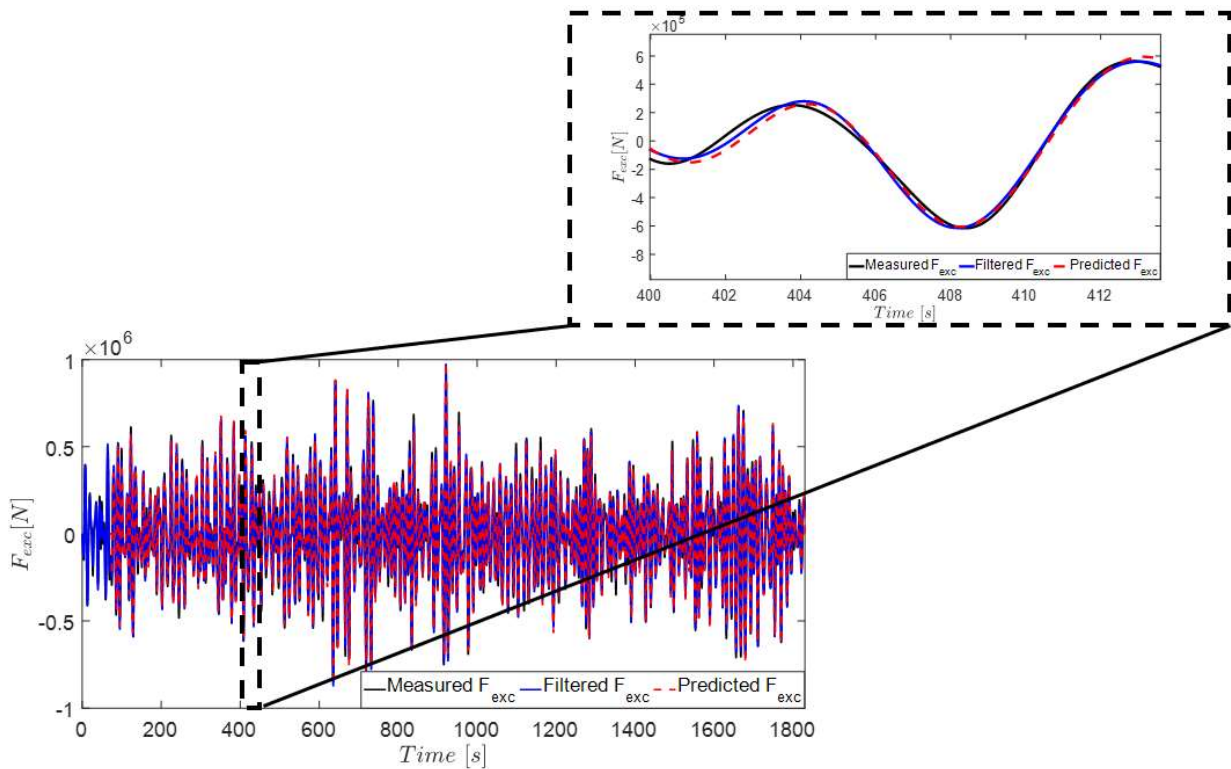


Figure 32  $N$ -step-ahead predicted and measured excitation force vs time,  $p = 250, N = 3500$ .

### 4.3 Estimation of Excitation Force

The Kalman Filter output includes position, velocity, and excitation force states. Figure 33 and Figure 34 show the position and velocity states output of KFHO for short time series (2 min), and both states are closely following the measured values which were given to the estimator.

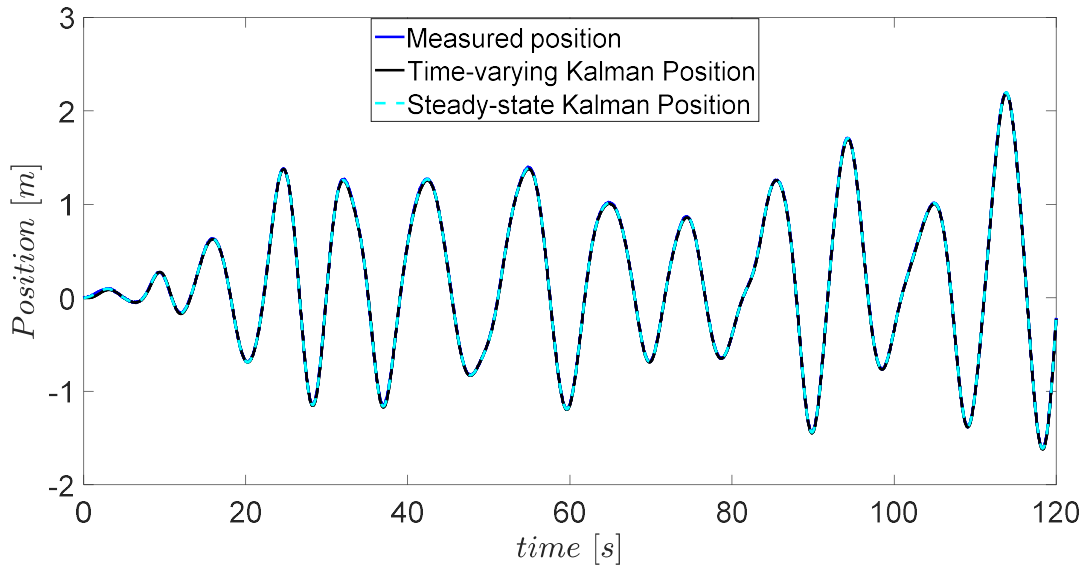


Figure 33 Measured position, Kalman estimated position, and Wave elevation vs time; measurement input from **nonlinear** system.

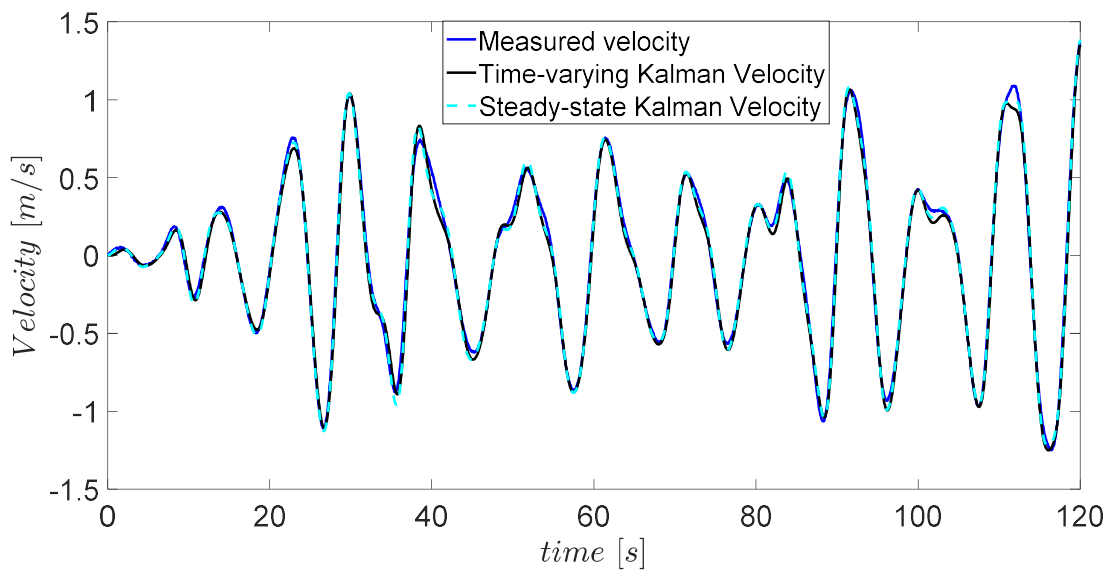


Figure 34 Measured velocity and Kalman estimated position vs time; measurement input from **nonlinear** system

The accuracy of the estimation of excitation force is reported by GoF for both time varying and steady-state KF and is shown for two cases where the measurements of excitation force are taken from linear and nonlinear plant as the input. In Figure 35, the estimation of excitation force is plotted along with the excitation force obtained from the simulation results (measured excitation force) of the nonlinear system. While, in Figure 36 estimated excitation force is plotted along the measured excitation force i.e. taken from linear system. In both cases, time varying KF gives better GoF than steady state. Besides, it is intuitively obvious that the linear KF has better GoF when it receives measurements from linear plant. These results are summarized in Table 4.

Lastly in Figure 37, the covariance of the estimation error of position over time is illustrated for time varying KF in order to check that the filter reaches steady state, i.e. expected when having stationary input noise.

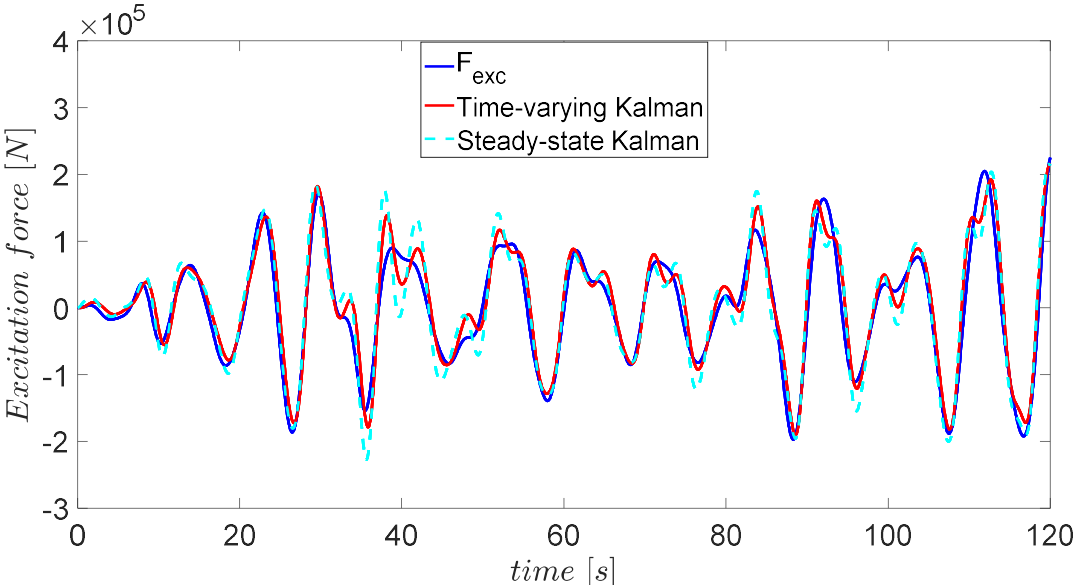


Figure 35 Measured and estimated excitation force of linear Kalman filter estimator; measurement input from **nonlinear** system

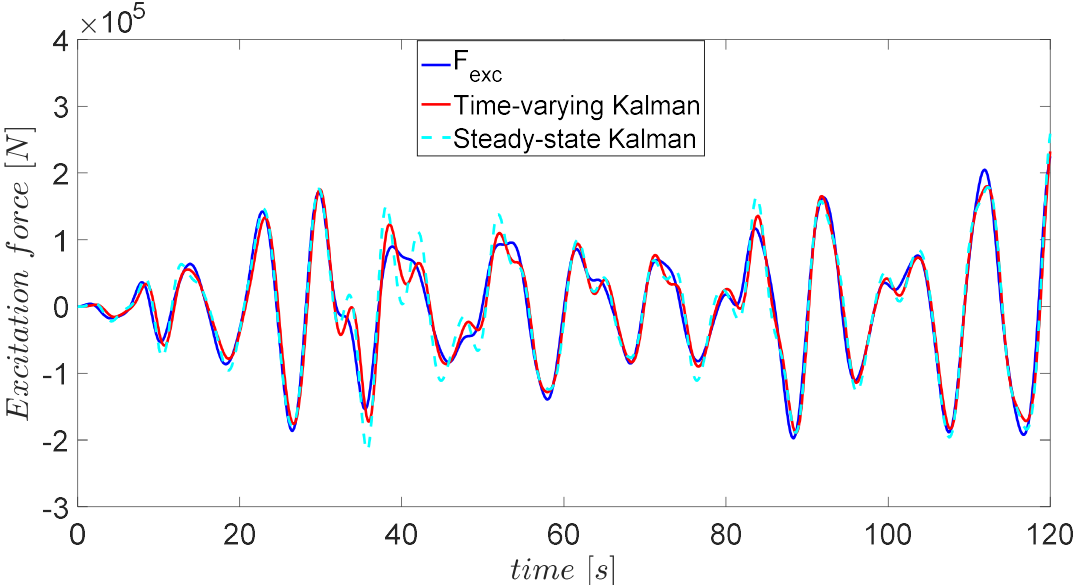


Figure 36 Measured and estimated excitation force of linear Kalman filter estimator; measurement input from **linear** system.

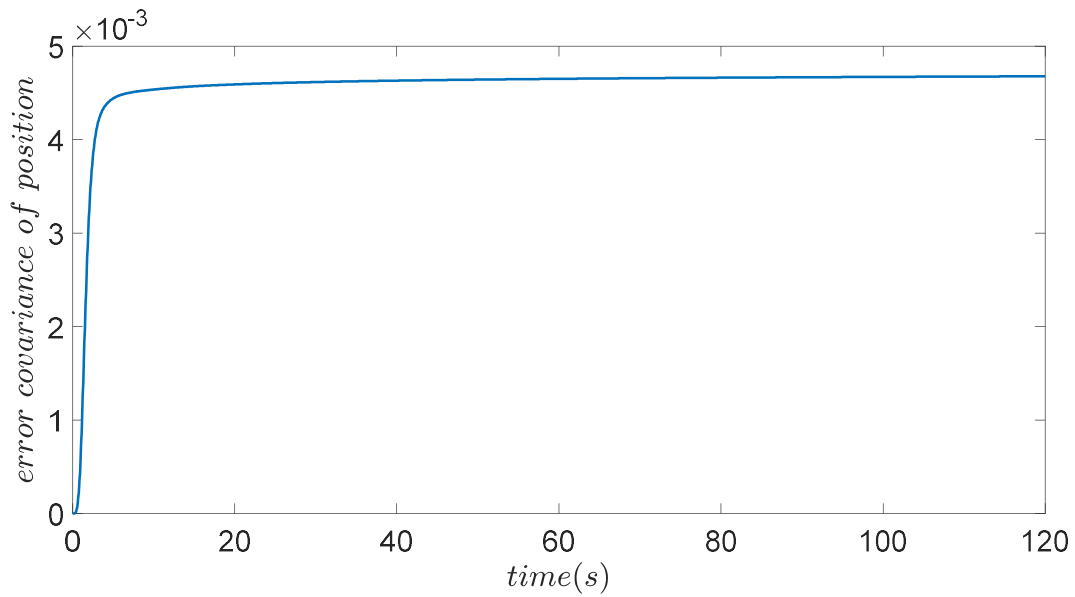


Figure 37 Covariance of the estimation error of position over time for time varying KF; measurement input from **nonlinear** system

Table 4 GoF for Time varying and Steady state KF for two cases where the measurements are obtained from linear or nonlinear system

<i>GoF</i>	Measurement from nonlinear plant	Measurement from linear plant
Time varying KF	73%	80.3%
Steady state KF	63.2%	74.4%

For further analysis and to verify the effect of the number of the frequencies that represent the dynamic of the excitation force, the GoF of the time varying and steady state Kalman Filter is reported for different number of frequencies in Table 5 for nonlinear plant.

Table 5 GoF for Time varying and Steady state KF for different frequency numbers,  $N_\omega$ , representing dynamic of the excitation force,  $T_h=5$  second.

<i>GoF</i>	Time varying KF	Steady state KF
$N_\omega = 201$	73.6%	71.4%
$N_\omega = 134$	73.4%	67.6%
$N_\omega = 81$	73%	63.2%
$N_\omega = 41$	72.2%	61.3%
$N_\omega = 17$	70.1%	67.3%
$N_\omega = 12$	67.6%	66.4%

## 4.4 Combining Prediction and Estimation of Excitation Force

Figure 38 and Figure 39 show the performance of the combined estimation and prediction of excitation force for prediction horizon of 5 second and 2.5 second which is compared against the measured value that is derived from the synthesized excitation force from nonlinear plant. The GoF for each process is summarized in Table 6 and Table 7. It is worth noting that the combination of prediction and estimation, the GoF vs Th does not have the same behavior compared to when looking at only AR performance.

The reason is by splitting the time series with Th and calculate the GoF for each horizon, the combined GoF changes and it can even decrease for low horizons.

*Table 6 GoF for combined prediction and estimation of excitation force, compared to filtered estimated excitation force*

<i>GoF</i>	<b>Predicted</b> compared to measured excitation force	<b>Predicted</b> compared to filtered estimated excitation force	<b>Filtered Estimated</b> compared to measured excitation force
<i>Th = 5s</i>	79.9%	96.6%	80.2%
<i>Th = 2.5s</i>	77.6%	99.4%	80.2%

*Table 7 GoF for combined prediction and estimation of excitation force, compared to estimated excitation force*

<i>GoF</i>	<b>Predicted</b> compared to measured excitation force	<b>Predicted</b> compared to estimated excitation force	<b>Estimated</b> compared to measured excitation force
<i>Th = 5s</i>	79.9%	74.6%	72.2%
<i>Th = 2.5s</i>	77.6%	71.1%	72.2%

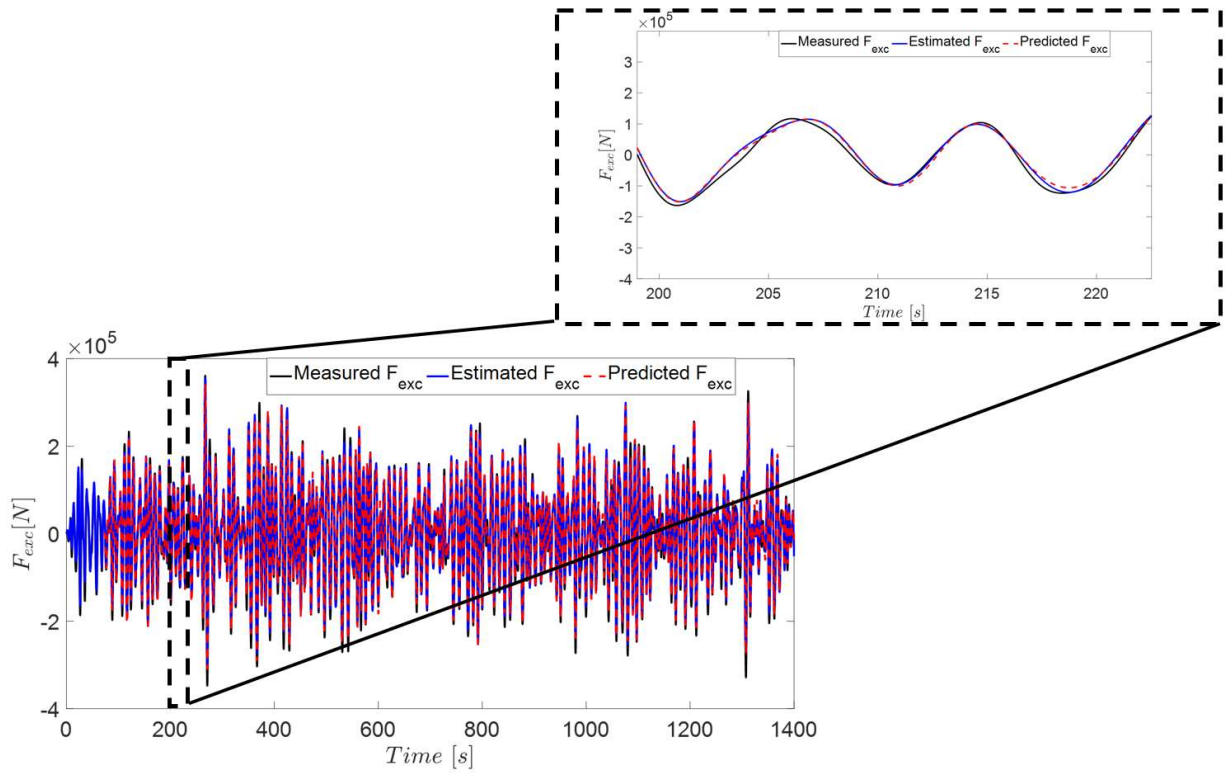


Figure 38 Comparing measured, estimated, and predicted excitation force, for  $p=250$ ,  $N=3500$ ,  $Th=5s$

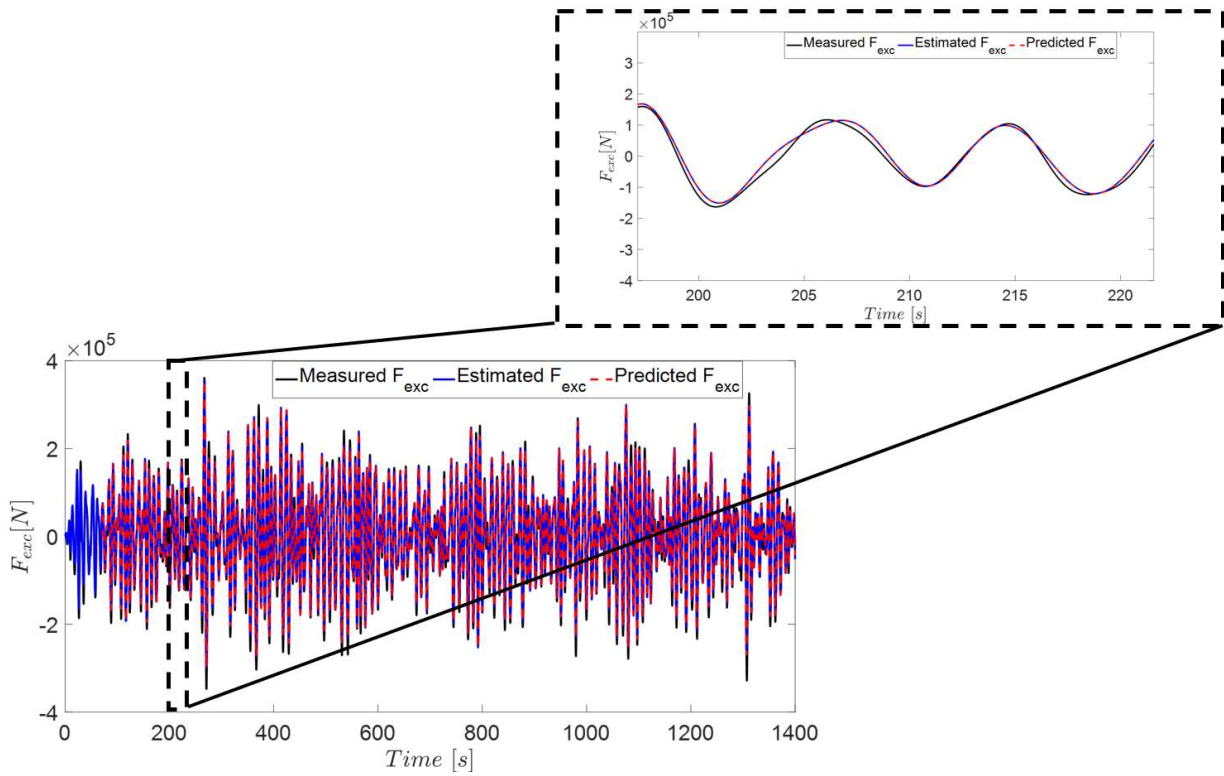


Figure 39 Comparing measured, estimated, and predicted excitation force, for  $p=250$ ,  $N=3500$ ,  $Th=2.5s$

## 5 DISCUSSION

---

### 5.1 Prediction Horizon

Filtering the transfer function decreased the noncausality of transfer function between the excitation force and velocity and hence, the prediction horizon falls within the range of predictability achievable with stochastic prediction methods such as AR predictors. Otherwise, in order to meet the prediction requirement, more complex prediction model and expensive instrumentation and more computational expensive model would be indispensable.

The critical parameter which affects the noncausality of the control system is the radiation resistance which is identified by the geometry of the buoy. As a result, different buoy designs imply different GoF for prediction horizon in similar sea states.

### 5.2 Prediction of Excitation Force

Several factors can affect the performance of the predictor model and revising them can result in increasing in the Goodness-of-fit between synthesized and predicted excitation force. The effect of each factors on AR predictor model is briefly discussed here.

The autoregressive model predicts the excitation force by a certain model order that has to be specified through optimization process. The higher order model provides the predictor with higher accuracy, however, the aliasing problem rises for higher model order, so the compromise should be taken to consideration.

The sampling time is another important factor that can influence the performance of predictor. Adequate sampling time not only prevents the predictor system from facing the aliasing problem, but also provides the system with the proper computational time by avoiding excessive computation.

In order to improve the performance of the predictor, a low pass filter has been applied to remove the high frequency content in the spectrum of excitation force. So, designing the low pass filter and choosing relevant cut off frequency according to the spectral density of excitation force can significantly increase the GOF. Recall that the real-time filter implementation needs to be further developed in order for the prediction model to be implemented in real time sea state. Since, in this work, the prediction of the excitation force is performed offline, which means the zero-phase delayed filter is assumed. In [2] is noted that in online operation of prediction, low pass filtering of the signal will introduce phase delay in system which results in reduction of accuracy of the predictor.

### 5.3 Estimation of Excitation Force

The accuracy of the estimation varies by changing the number of frequencies and the variance value of the covariance matrices of process and measurement noise.

Increasing the number of frequencies provides the time varying KFHO with more accurate result, however, the GoF seems to converge to a certain value when increasing the frequencies number. The steady-state KFHO shows a random behavior for GoF in contrast to the time varying filter.

On the other hand, this increase in the number of frequencies resulted in facing a more computational expensive problem. Therefore, the optimal value for required number of frequencies should be taken.

The disturbance value of the excitation force (process noise) affects the amplitude of estimated excitation force and the disturbance should be similar in the order magnitude to the excitation force. Zero disturbance will lead to zero output from the system since the system remains in its equilibrium position. The variance of the noise depends on the sensor properties as well as operating wave condition of the WEC. It has been set as an approximate value based on the wave elevation.

In this work, the frequency matrix is considered fixed, while considering a time varying frequency matrix results in nonlinearity which should be solved by nonlinear Kalman filter system such as EKF estimator, as it is discussed in [24].

## **5.4 Combining Prediction and Estimation of Excitation Force**

The combined prediction and estimation of excitation force for time horizon of 2.5 second shows slightly lower accuracy comparing to time horizon of 5 second. However, the accuracy of the former prediction process is significantly higher than the latter when considering the GoF of prediction compared to estimated excitation force. It can hence be concluded that the accuracy for the total prediction and estimation process is limited by the estimation process.

## 6 CONCLUSION

---

This research investigates a methodology to estimate and predict the excitation force by the aid of the autoregressive model as predictor and Kalman Filter as estimator. The performance of each process is discussed through separate sections and the combined accuracy of all methods is discussed for a given sea state.

Defining the prediction horizon is the center topic in real time control of the WEC and plays an important role for predicting the excitation force in order to improve the energy extraction of wave energy converters. The required prediction horizon has been derived based on suboptimal and optimal control velocity of the buoy for which the geometry of the buoy shows a significant influence on the computation of prediction horizon.

Further on, the prediction of excitation force has been carried out by the use of AR predictor. The influence of several predictor parameters has been investigated to improve Goodness-of-fit of the predicted excitation force compared to synthesized excitation force. It is also discussed the effect of low pass filtering on improving the prediction of signals by removing the high frequency contents which displays drastic improvement in GoF. Considering all optimizations, AR model predictor provides an accurate future knowledge, that is needed to be implemented into the control strategy to optimize the energy capture of the WEC.

Then, the implemented Kalman Filter with harmonic oscillator in combination with the linearized system model successfully estimates the excitation force by only measuring the position and velocity of the WEC. The performance of steady-state and time-varying KFHO has been compared, when the time-varying approach expresses better accuracy of estimation. It has been seen that choosing an optimum number of frequencies, for identification of the excitation force dynamic, and covariance matrices of the process and measurement noise, have a major effect on the accuracy of the estimation.

Finally, the validity of the prediction, estimation and prediction horizon methods has been confirmed through combining these methods for a given sea state. Comparing the results of the prediction process and the one from combined prediction and estimation, it has been seen that the GoF from combined process is only slightly lower than the GoF from estimation process. In other words, predicted excitation force closely follows the estimated excitation force specially with prediction horizon of 2.5 second. Therefore, the most error stemmed from the estimation process.

The methods that have been used in this work will be implemented in power maximizing strategies of CorPower Ocean WEC control model.

## 7 FUTURE WORK

---

### 7.1 Prediction Horizon

Knowing that the geometry of the buoy has significant influence on the radiation resistance, it would be interesting to investigate the effect of geometrical parameters on the prediction horizon.

Moreover, the presented method filters the transfer function based on the dominant frequency content of excitation force, and therefore it would be of future work to compare the energy capture between the filtered and non-filtered transfer function and estimate the loss.

### 7.2 Prediction of Excitation Force

Least square method is one of several ways to identify the AR model coefficients, however, different methods can be used to minimize the cost function such as Yule-Walker, Berg, and Hannan-Rissanen. It would be valuable to compare the obtained regression coefficients and check the effect of that on predictor performance.

The AR coefficients are also assumed to be constant throughout the prediction horizon, while in real sea state with longer data set, a model with updated coefficients needs to be implemented when sea state changes. Hence, it would be of interest to investigate the performance of such predictor with varying regression coefficients.

### 7.3 Estimation of Excitation Force

In order to improve the accuracy of the estimation, a time varying Kalman Filter can be used in which the systems matrices are updated along with estimation of each time step. For this purpose, Taylor expansion can be performed for linearization of the forces at each time step, and hence, the resulting behavior will be closer to the non-linear nature of the forces.

Moreover, the dynamic model of the excitation force can be improved by assuming the excitation force as a linear superposition of a limited number of harmonic oscillators where the amplitude, phase, and frequency of each component of  $F_{exc}$  should be estimated as it is discussed in [20] and it is briefly explained in [11] as Extended Kalman Filter Harmonic oscillator, EKFHO.

$$F_{exc} = \sum_{i=1}^n A_i \cos(\omega_i t + \phi_i) \quad (7.1)$$

## REFERENCES

---

1. Xie, Lihua, Dan Popa, and Frank L. Lewis. Optimal and robust estimation: with an introduction to stochastic control theory. CRC press, 2007.
2. Garcia-Abril, M., F. Paparella, and J. V. Ringwood. "Excitation force estimation and forecasting for wave energy applications." *IFAC-PapersOnLine* 50.1 (2017): 14692-14697.
3. Korde, Umesh A., and John Ringwood. *Hydrodynamic control of wave energy devices*. Cambridge University Press, 2016.
4. Pena-Sanchez, Yerai, and John V. Ringwood. "A critical comparison of AR and ARMA models for short-term wave forecasting." *Proc. 12th Eur. Wave Tidal Energy Conf.* 2017.
5. Falnes, Johannes. Ocean waves and oscillating systems: linear interactions including wave-energy extraction. Cambridge university press, 2002.
6. Price, A. A. E., D. I. M. Forehand, and A. R. Wallace. "Time-span of future information necessary for theoretical acausal optimal control of wave energy converters." *2009 European Control Conference (ECC)*. IEEE, 2009.
7. Peña-Sanchez, Yerai, et al. "Estimation and forecasting of excitation force for arrays of wave energy devices." *IEEE Transactions on Sustainable Energy* 9.4 (2018): 1672-1680.
8. Reid, Ian, and Hilary Term. "Estimation ii." *University of Oxford, Lecture Notes* (2001).
9. Todalshaug, J. H. et al. "Control model of the CorPower WEC to be used for optimization purposes." Internal memo. Unpublished, 2018.
10. Stutts, Daniel S. "Equivalent viscous damping." (2009).
11. Peña-Sanchez, Yerai, et al. "A critical comparison of excitation force estimator for wave energy devices." *Submitted to IEEE Trans. on Control Systems Technology*, 2019.
12. Falnes, Johannes. "On non-causal impulse response functions related to propagating water waves." *Applied Ocean Research* 17.6 (1995): 379-389.
13. Falnes, Johannes. "A review of wave-energy extraction." *Marine structures* 20.4 (2007): 185-201.
14. MathWorks, (2019). Control System Toolbox: User's Guide (R2016a). Retrieved May 26, 2019 from <https://se.mathworks.com/help/control/ug/kalman-filtering.html>
15. Guo, Bingyong, et al. "Numerical and experimental studies of excitation force approximation for wave energy conversion." *Renewable Energy* 125 (2018): 877-889.
16. Abdelrahman, Mustafa, et al. "Estimation of wave excitation force for wave energy converters." *2016 3rd Conference on Control and Fault-Tolerant Systems (SysTol)*. IEEE, 2016.
17. Kracht, Peter, et al. "Performance improvement of a point absorber wave energy converter by application of an observer-based control: Results from wave tank testing." *IEEE Transactions on Industry Applications* 51.4 (2015): 3426-3434.
18. Ling, Bradley A. "Real-time estimation and prediction of wave excitation forces for wave energy control applications." (2015).

19. Fusco, Francesco, and John V. Ringwood. "A simple and effective real-time controller for wave energy converters." *IEEE Transactions on sustainable energy* 4.1 (2013): 21-30.
20. Mhatre, Sanil. Application of a Linear Optimal Estimator on a Wave Energy Converter Using Bang-Singular-Bang Control. Diss. Michigan Technological University, 2017.
21. Nguyen, H-N., and Paolino Tona. "Wave excitation force estimation for wave energy converters of the point-absorber type." *IEEE Transactions on Control Systems Technology* 99 (2017): 1-9.
22. Scruggs, J. T., et al. "Optimal causal control of a wave energy converter in a random sea." *Applied Ocean Research* 42 (2013): 1-15.
23. Mérigaud, Alexis, and John V. Ringwood. "Incorporating ocean wave spectrum information in short-term free-surface elevation forecasting." *IEEE Journal of Oceanic Engineering* 99 (2018): 1-14.
24. Fusco, Francesco, and John V. Ringwood. "Short-term wave forecasting for real-time control of wave energy converters." *IEEE Transactions on sustainable energy* 1.2 (2010): 99-106.
25. Paparella, Francesco, et al. "Benefits of up-wave measurements in linear short-term wave forecasting for wave energy applications." *2014 IEEE Conference on Control Applications (CCA)*. IEEE, 2014.
26. Ge, Ming, and Eric C. Kerrigan. "Short-term ocean wave forecasting using an autoregressive moving average model." *2016 UKACC 11th International Conference on Control (CONTROL)*. IEEE, 2016.
27. Schoen, Marco P., Jørgen Hals, and Torgeir Moan. "Wave prediction and robust control of heaving wave energy devices for irregular waves." *IEEE Transactions on energy conversion* 26.2 (2011): 627-638.
28. Price, A. A. E., and A. R. Wallace. "Non-linear methods for next wave estimation." *Proceedings of the 7th European Wave and Tidal Energy Conference, Porto*. (2007).
29. Zhou, Tianzhi. "Damping Profile Research for CorPower Ocean's Wave Energy Converter." (2016).
30. Retrieved May 29, 2019 from <http://www.corpowerocean.com/>
31. Ljungbäck, Jacob. "Characterization of cascade gearbox for wave energy converter." (2015).
32. Göteman, Malin. "Wave power from energy source to wave power systems", *in press*. (2019).
33. Mathworks. (2019). *Control System Toolbox: User's Guide (r2016b)*. Retrieved May 26, 2019 from <https://se.mathworks.com/help/control/ug/kalman-filtering.html>
34. Retrieved May 29, 2019 from <https://se.mathworks.com/help/physmod/simscape/ref/translationalfriction.html>

# APPENDIX A

Budal diagram shows that  $P_A$  has increasing trend, since the immersed body volume is sufficiently large ( $V \rightarrow \infty$ ), and in some articles, it is called the amount of available power by ocean. Furthermore,  $P_B$  has declining trend since the immersed body volume is sufficiently small ( $V \rightarrow 0$ ), and it is also called the amount of possible power by the wave energy converter. Figure below shows the Budal for which the power absorbed by latching (active) and passive control system is illustrated.[13]

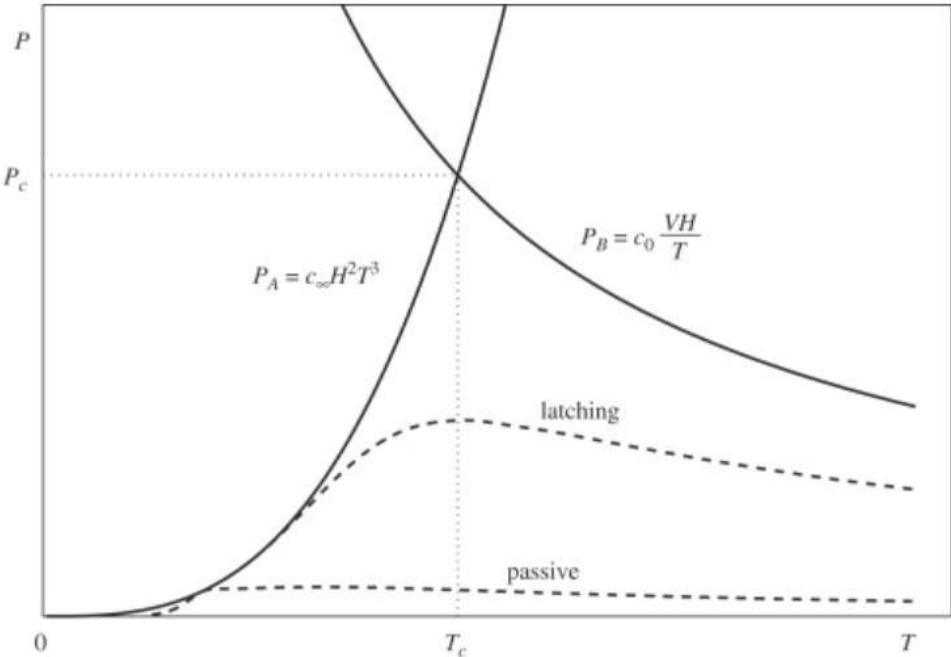


Figure A.1 Budal Diagram. Adapted from “A review of wave-energy extraction” Johannes Falnes, 2007, *Marine structures*, 20, p. 191.

## APPENDIX B

From mathematical point of view, the friction force can express as; [34]

$$F_f = (F_C + F_S e^{-c_s |v|}) \text{sign}(v) + c_v v \quad |v| \geq v_{th} \quad (B.1)$$

$$F_f = \frac{v(c_v v_{th} + F_C + F_S e^{-c_s v_{th}})}{v_{th}} \quad |v| < v_{th} \quad (B.2)$$

Where,  $v_{th}$  is the threshold velocity,  $F_S$  is the Stribeck force, and  $F_C$  is the Coulomb force. Which the sum of the Coulomb and Stribeck Force constant represent the breakaway force;

$$F_{brk} = F_C + F_S \quad (B.3)$$

The Coulomb friction, Stribeck friction and, viscous friction is proportional to the normal load. The Stribeck curve can be presented as below;

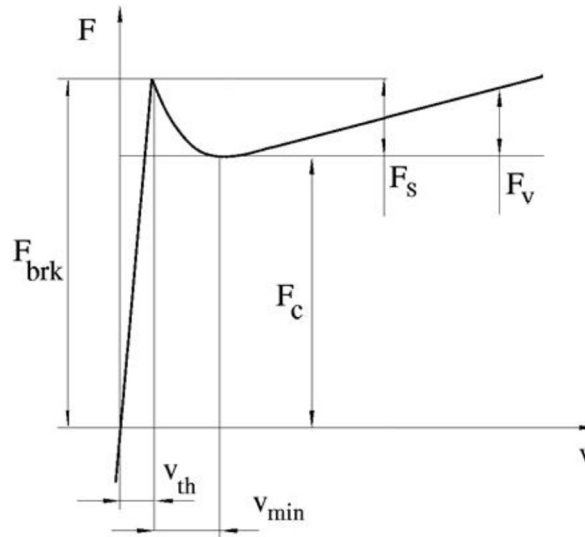


Figure B.1 The Stribeck friction curve representing the breakaway friction, Coulomb friction, and viscous friction.

Retrieved May 29, 2019 from

<https://se.mathworks.com/help/physmod/simscape/ref/translationalfriction.html>

In the CorPower Ocean model, normal load,  $N$ , can be introduced for pulleys and some other component. Furthermore, the constant force,  $F_C$  and  $F_S$ , can be replaced by the product of friction coefficient,  $f_C$  and  $f_S$ , and normal force  $N$ ;

$$F_C = f_C N \quad F_S = f_S N \quad (B.4)$$

So, the friction forces of pneumatic cylinders and bearings for CorPower ocean model is expressed as follows;

$$F_f = N(f_C + f_S e^{-c_s |v|}) \text{sign}(v) + N f_v v \quad |v| \geq v_{th} \quad (B.5)$$

$$F_f = vN(f_v v_{th} + f_C + f_S e^{-c_s v_{th}})/v_{th} \quad |v| < v_{th} \quad (B.6)$$